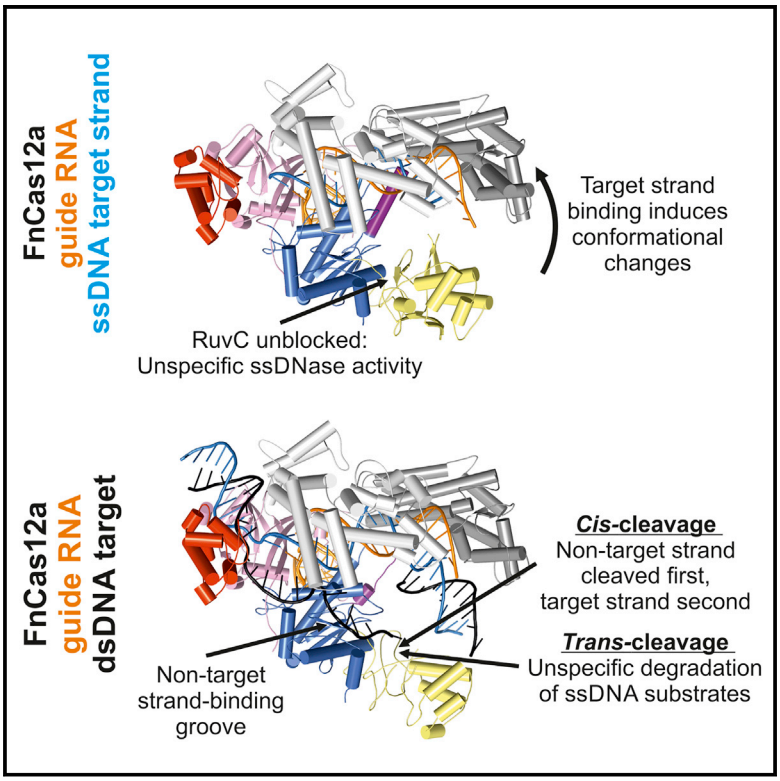
Article

Molecular Cell

Mechanistic Insights into the *cis*- and *trans*-Acting DNase Activities of Cas12a

Graphical Abstract



Highlights

- Target ssDNA binding allosterically induces unblocking of the RuvC active site
- PAM binding facilitates strand separation in dsDNA targets
- Non-target DNA strand cleavage precedes target DNA strand cleavage
- Cas12a releases the PAM-distal end of cleaved dsDNA targets

Authors

Daan C. Swarts, Martin Jinek

Correspondence

jinek@bioc.uzh.ch

In Brief

Swarts et al. elucidated two structures of Cas12a in complex with a guide RNA and with either single-stranded or double-stranded DNA targets. Together with biochemical assays, these structures reveal the mechanisms of Cas12a-mediated *cis* and *trans* cleavage of DNA substrates.

Swarts & Jinek, 2019, Molecular Cell *73*, 589–600
February 7, 2019 © 2018 Elsevier Inc.
https://doi.org/10.1016/j.molcel.2018.11.021

CellPress

Molecular Cell
Article

Mechanistic Insights into the *cis*- and *trans*-Acting DNase Activities of Cas12a

Daan C. Swarts[1] and Martin Jinek[1,2,*]
[1]Department of Biochemistry, University of Zurich, 8057 Zurich, Switzerland
[2]Lead Contact
*Correspondence: jinek@bioc.uzh.ch
https://doi.org/10.1016/j.molcel.2018.11.021

SUMMARY

CRISPR-Cas12a (Cpf1) is an RNA-guided DNA-cutting nuclease that has been repurposed for genome editing. Upon target DNA binding, Cas12a cleaves both the target DNA in *cis* and non-target single-stranded DNAs (ssDNAs) in *trans*. To elucidate the molecular basis for both DNase cleavage modes, we performed structural and biochemical studies on *Francisella novicida* Cas12a. We show that guide RNA-target strand DNA hybridization conformationally activates Cas12a, triggering its *trans*-acting, non-specific, single-stranded DNase activity. In turn, *cis* cleavage of double-stranded DNA targets is a result of protospacer adjacent motif (PAM)-dependent DNA duplex unwinding, electrostatic stabilization of the displaced non-target DNA strand, and ordered sequential cleavage of the non-target and target DNA strands. Cas12a releases the PAM-distal DNA cleavage product and remains bound to the PAM-proximal DNA cleavage product in a catalytically competent, *trans*-active state. Together, these results provide a revised model for the molecular mechanisms of both the *cis*- and the *trans*-acting DNase activities of Cas12a enzymes, enabling their further exploitation as genome editing tools.

INTRODUCTION

In prokaryotes, CRISPR-Cas systems function as programmable immune systems that utilize CRISPR RNAs (crRNAs) as guide molecules for the recognition and targeting of invasive nucleic acids, such as viral DNA (Koonin et al., 2017; Mohanraju et al., 2016). The DNA targeting class 2 CRISPR-Cas systems, which comprise types II and V, elicit antiviral immunity by means of single multidomain nuclease enzymes that mediate crRNA-guided target DNA binding and catalyze target DNA cleavage. Cas9 and Cas12a proteins, the respective effector nucleases of type II and type V-A systems, mediate crRNA-guided DNA cleavage by recognizing two distinct sequence elements in the target DNA: (1) a "protospacer" sequence, specified by Watson-Crick base-pairing interactions with the crRNA and (2) a protospacer adjacent motif (PAM), recognized via sequence- and/or shape-specific protein-DNA interactions (Swarts and Jinek, 2018). Upon binding of a cognate target DNA, the complementary spacer-derived segment of the crRNA and the protospacer "target strand" (TS) form an RNA-DNA heteroduplex. At the same time, the non-target strand (NTS) of the protospacer is displaced. Formation of this so-called "R-loop" structure catalytically activates both Cas9 and Cas12a, triggering *cis* cleavage of both target DNA strands. The ability to program Cas9 and Cas12a with a guide RNA of choice has led to their repurposing for precision genome editing and for regulation of gene expression (Barrangou and Doudna, 2016; Swarts and Jinek, 2018; Wang et al., 2016; Wright et al., 2016).

Despite similar functionalities, Cas9 and Cas12a proteins have distinct evolutionary histories and therefore distinct mechanistic properties (Shmakov et al., 2017; Swarts and Jinek, 2018). *Streptococcus pyogenes* Cas9, which is widely used for genome editing, recognizes a 5′-NGG-3′ PAM directly downstream of the protospacer NTS (Anders et al., 2014). In contrast, Cas12a orthologs used for genome editing recognize a 5′-TTTV-3′ PAM directly upstream of the protospacer NTS (Gao et al., 2016; Sun et al., 2018; Świat et al., 2017; Tu et al., 2017; Yamano et al., 2016; Zetsche et al., 2015). However, Cas12a can also target DNAs with "suboptimal" PAMs (5′-TTV-3′, 5′-TCTV-3′, 5′-TCCV-3′, and 5′-CCCV-3′), albeit often at lower efficiencies (Gao et al., 2017; Nishimasu et al., 2017; Tu et al., 2017; Yamano et al., 2017). Cas9 and Cas12a furthermore use different mechanisms for DNA cleavage. Cas9 cleaves the TS and NTS with its HNH and RuvC domains, respectively (Gasiunas et al., 2012; Jinek et al., 2012). This typically results in PAM-proximal double-strand DNA breaks (DSBs) with blunt ends or 1-nt overhangs. In contrast, Cas12a uses a single RuvC nuclease domain for cleavage of both strands of the target DNA (Swarts et al., 2017), generating PAM-distal DSBs with larger (5–7 nt) 5′ overhangs (Zetsche et al., 2015). Although both Cas9 and Cas12a initially cleave a target double-stranded DNA (dsDNA) at a single site, both enzymes catalyze trimming of the cleaved target ends *in vitro* (Jinek et al., 2012; Stephenson et al., 2018), yielding heterogeneous cleavage products. Finally, Cas12a exhibits two distinct DNA cleavage modes (Chen et al., 2018; Li et al., 2018). Besides cleaving dsDNA targets in a crRNA-guided manner in *cis*, Cas12a also possesses sequence-independent DNase activity that cleaves non-target, single-stranded DNA in *trans* (Chen et al., 2018; Li et al., 2018). The *trans*-acting nuclease

activity is triggered by hybridization of the crRNA to a complementary target DNA strand (Chen et al., 2018; Li et al., 2018).

Structural studies of Cas12a have revealed its overall molecular architecture and mechanism of target DNA recognition. The enzyme has a bilobed architecture, in which the N-terminal REC lobe, consisting of the α-helical domains REC1 and REC2, is connected by the wedge (WED) domain to the C-terminal NUC lobe comprising the PAM-interacting (PI), bridge helix (BH), RuvC, and Nuc dmains (Dong et al., 2016; Gao et al., 2016; Stella et al., 2017; Swarts et al., 2017; Yamano et al., 2016). The crRNA is recognized via sequence- and shape-specific interactions with the repeat-derived part of the crRNA, which forms a pseudoknot structure (Dong et al., 2016). crRNA binding results in structural pre-ordering of the seed segment in the crRNA, thereby priming the Cas12-crRNA complex for target DNA recognition (Swarts et al., 2017). Shape- and sequence-specific recognition of the PAM then facilitates target dsDNA binding and is prerequisite for catalyzing DNA cleavage (Gao et al., 2016; Yamano et al., 2016; Zetsche et al., 2015). Despite these insights, the molecular mechanisms underpinning *cis*- and *trans*-acting DNase activities of Cas12a have remained unclear.

To obtain insights into both *cis*- and *trans*-acting DNA cleavage activities of Cas12a, we have determined the crystal structures of *Francisella novicida* U112 Cas12a (FnCas12a) in ternary complexes with a crRNA and either single-stranded DNA (ssDNA) or dsDNA targets. Together with corroborating biochemical experiments, the structure of Cas12a bound to a guide crRNA and ssDNA target reveals that crRNA-TS DNA duplex formation, rather than PAM binding, drives a conformational rearrangement that allosterically activates the Cas12a RuvC domain. Although PAM binding does not play a role in the catalytic activation of Cas12a, it is essential for the recognition and cleavage of dsDNA targets because it promotes dsDNA strand separation and consequently R-loop formation. The crystal structure of Cas12a-crRNA in complex with a dsDNA target reveals that the NTS of the target DNA is electrostatically guided toward the catalytic site in the RuvC domain, thus facilitating sequential cleavage of the NTS and TS DNA strands. We furthermore demonstrate that, after target DNA cleavage by Cas12a, the PAM proximal-DNA cleavage product remains bound to the Cas12a-crRNA complex, which maintains Cas12a in a catalytically activated state and enables degradation of non-target ssDNA in *trans*.

RESULTS

Target ssDNA Binding Allosterically Activates the RuvC Catalytic Site in Cas12a

In addition to cleaving target dsDNAs in *cis*, Cas12a enzymes were recently reported to possess *trans* DNA cleavage activity triggered by target ssDNA binding (Chen et al., 2018; Li et al., 2018). To corroborate these findings, we programmed *Francisella novicida* Cas12a (FnCas12a) with a crRNA and incubated the resulting complex with circular ssDNA (M13 ssDNA) or circular dsDNA (M13 dsDNA) substrates that bear no complementarity to the crRNA. Next, we added to the reaction 20-nt ssDNA oligonucleotides that lacked a PAM and were either fully complementary or lacked complementarity to the spacer-derived segment of the crRNA (Figure 1A). In the presence of a non-complementary ssDNA, FnCas12a did not degrade the M13 DNAs. In contrast, the presence of a complementary target ssDNA caused complete FnCas12a-mediated degradation of M13 ssDNA, but not M13 dsDNA (Figure 1B). This activity was not observed for the RuvC catalytic site mutant FnCas12a^{E1006Q}, indicating that the observed in *trans* cleavage of ssDNA substrates is mediated by the RuvC catalytic site that also mediates canonical *cis* cleavage of target dsDNA. These findings are in agreement with the previously reported *trans*-acting activity of Cas12a (Chen et al., 2018; Li et al., 2018) and, as a PAM is absent from the *trans*-activating ssDNA, suggest that crRNA-TS hybridization alone drives allosteric activation of Cas12a.

To obtain structural insights into the allosteric mechanism underpinning catalytic activation of Cas12a, we determined the crystal structure of a ternary complex consisting of FnCas12a bound to a crRNA guide and a 20-nt PAM-less target ssDNA (FnCas12a-crRNA-ssDNA complex) (Figures 1C, 1D, and S1) at a resolution of 2.98 Å (Table 1). In agreement with other Cas12a structures, the FnCas12a-crRNA-ssDNA complex maintains a bilobed architecture. The first 20 nt of the spacer-derived segment of the crRNA (A1-U20) form Watson-Crick base pairs with the TS, and the 3′-terminal nucleotides of the crRNA (U22-G24) are structurally disordered. Previously determined structures of binary Cas12a-crRNA complexes (PDB: 5NG6 and PDB: 5ID6) showed that the REC2 domain occludes the catalytic site in the RuvC domain (Figure 1E), which likely prevents not only *cis* cleavage of target dsDNA but also *trans* cleavage of non-target ssDNAs. This is consistent with the observed lack of *trans*-acting nuclease activity in the absence of a *trans*-activating target DNA (Figure 1B).

Although both ssDNA and dsDNA target binding induced cleavage of the M13 ssDNA substrate in *trans*, neither target DNA was able to trigger *trans* cleavage of M13 dsDNA (Figure 1B). We previously modeled the binding of an ssDNA substrate in the RuvC catalytic site based on superpositions with the structures DNA-bound complexes of Cas12b (Swarts et al., 2017). In agreement with the *trans* cleavage experiments, modeling of a dsDNA substrate reveals that the RuvC catalytic site cannot accommodate a B-form DNA duplex (PDB: 1BNA), due to severe steric clashes of both dsDNA strands with the RuvC domain (Figure 1F). Consequently, this implies that *cis* cleavage of a dsDNA target requires that the dsDNA is unwound to allow sequential cleavage of TS and NTS strands in the RuvC active site.

Structural superposition of the binary FnCas12a-crRNA (PDB: 5NG6) and ternary FnCas12a-crRNA-ssDNA complex structures reveals the conformational changes associated with catalytic activation upon TS binding (Figures 1E and S2; root-mean-square deviation [RMSD]: 12.54 Å). The NUC lobe is largely unperturbed by TS binding (RMSD of NUC lobe alignment: 2.61 Å), with only a small rotation of the Nuc domain by ~9° relative to the remainder of the NUC lobe. In contrast, the REC lobe undergoes a major conformational rearrangement (RMSD of REC lobe alignment: 15.26 Å). The REC1 domain rotates approximately 33° relative to the NUC lobe and thereby moves closer to the NUC lobe and to the crRNA-TS heteroduplex (Figure S2B),

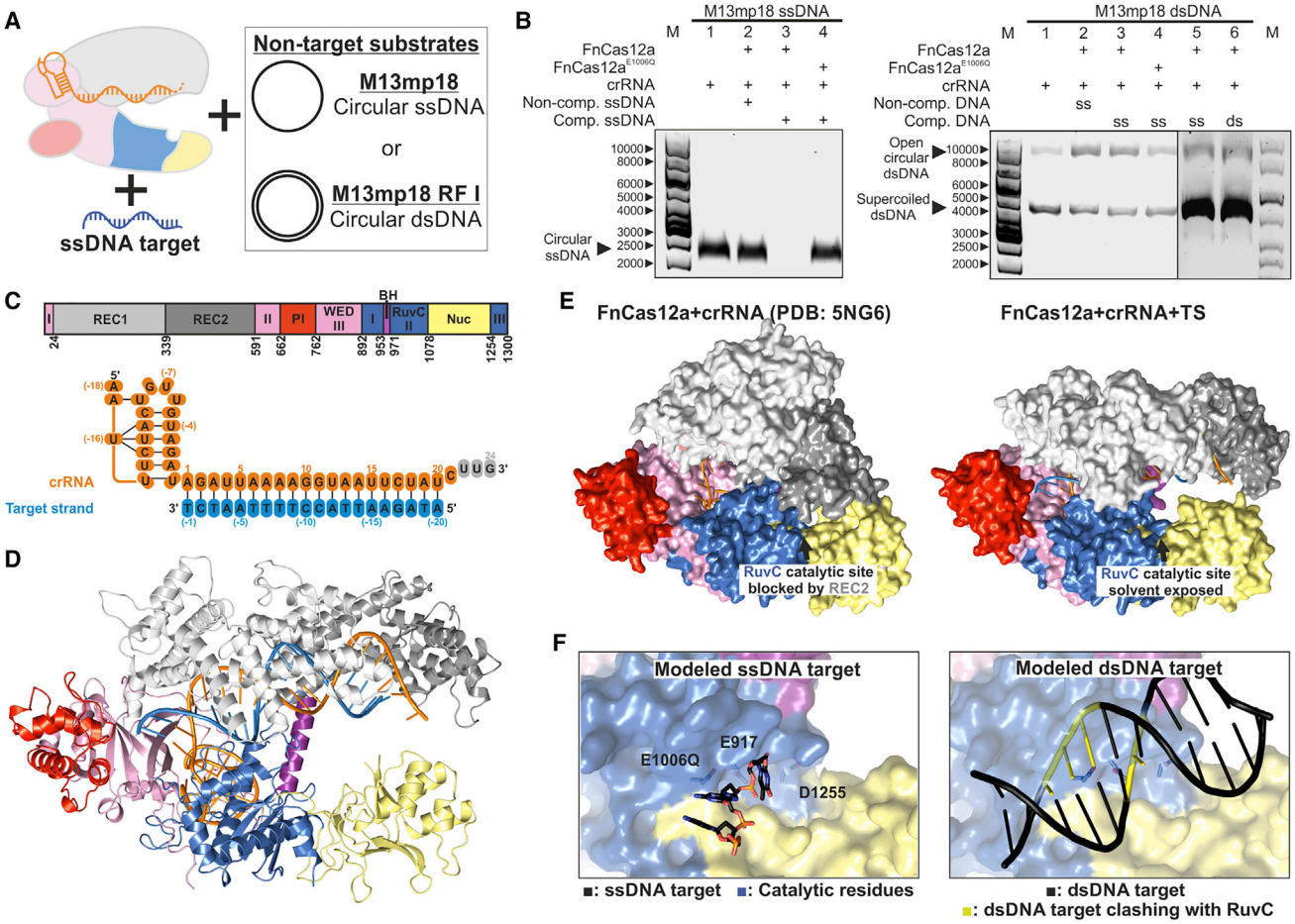


Figure 1. Target ssDNA Binding Allosterically Activates the RuvC Catalytic Site in Cas12a

(A) Schematic diagram of experiments investigating FnCas12a-mediated *trans* cleavage of M13 DNA.

(B) (Left and right) Non-target circular M13 ssDNA (left panel) or circular M13 dsDNA (right panel) substrates were incubated with FnCas12a-crRNA in the presence or absence of (non-)complementary ssDNA (ss) or dsDNA (ds) targets. Degradation products were resolved by agarose gel electrophoresis. Comp., complementary; ds, double-stranded; M, 1-kb DNA ladder marker; ss, single-stranded.

(C) (Top) Schematic diagram of the domain organization of FnCas12a. BH, bridge helix; Nuc, nuclease; PI, protospacer adjacent motif (PAM) interacting; REC, recognition; WED, wedge. Both the WED and RuvC domains are formed by three discontinuous segments of the protein sequence. (Bottom) Sequence of the crRNA guide and TS DNA (see also Table S1) in the structure of the FnCas12a-crRNA-TS complex is shown (see also D). Structurally disordered crRNA nucleotides are colored gray.

(D) Overall structure of the FnCas12a-crRNA-TS complex. Domains are colored according to the scheme in (C). For details of FnCas12a-crRNA-TS binding interactions, see Figure S1.

(E) Surface representation of the binary FnCas12a-crRNA (PDB: 5NG6) and the ternary FnCas12a-crRNA-TS DNA complex structures. Domains are colored according to the scheme in (C). See Figure S2 for additional structural comparisons.

(F) Models of DNA substrates bound in the activated catalytic site of FnCas12a. (Left) A single-stranded target DNA modeled in the RuvC catalytic site of FnCas12a (PDB: 5NFV) is shown. The modeled DNA is based on superposition of the structure of AacCas12b-crRNA bound to a DNA target (PDB: 5U33). (Right) A dsDNA (PDB: 1BNA) modeled in the RuvC catalytic site of FnCas12a (PDB: 5NFV) is shown. Nucleotides that sterically clash with the FnCas12a RuvC domain are colored yellow.

allowing formation of stabilizing interactions between the crRNA-TS heteroduplex and REC1 (Figure S1). The REC2 domain undergoes a rotation of 46° and a translation of ~9.5 Å relative to the REC1 domain. This is essential to accommodate the PAM-distal end of the crRNA-TS heteroduplex, which would otherwise result in severe clashes with the REC2 domain (Figure S1C). In addition, the rearrangement results in the formation of stabilizing interactions between the crRNA-TS heteroduplex and REC2 residues (Figure S1).

To investigate conformational differences between ternary structures bound to either ssDNA or dsDNA targets, we superimposed the structure of the FnCas12a-crRNA-TS complex and previously determined ternary structures of FnCas12a-crRNA complexes bound to intact (PDB: 5MGA) and cleaved (PDB: 5NFV) dsDNA targets (Figures S2C and S2D). The structure of the FnCas12a-crRNA-ssDNA complex is most similar to that of the cleaved dsDNA-bound complex (RMSD: 2.76 Å; Figure 2C). We observe minor narrowing of the PI domain in which the

Table 1. Crystallographic Data Collection and Refinement Statistics

Dataset	TS-Only Complex	Ternary R-Loop Complex
FnCas12a	WT	E1006Q
RNA	crRNA1	crRNA1
DNA	oDS311 (TS)	oDS142 (TS) + oDS141 (NTS)
X-ray source	SLS PXIII	SLS PXIII
Space group	$P2_1\ 2_1\ 2_1$	$P1\ 2_1\ 1$
Cell Dimensions		
a, *b*, *c* (Å)	78.80, 188.58, 284.12	82.17, 141.68, 89.48
α, β, γ (°)	90, 90, 90	90, 97.43, 90
Wavelength (Å)	1	1.008
Resolution (Å)[a]	48.67–2.98 (3.09–2.98)	47.61–2.65 (2.75–2.65)
R_{meas} (%)[a]	18.09 (189.7)	8.18 (190.8)
CC1/2 (%)	0.999 (0.675)	1 (0.638)
$I/\sigma I$[a]	18.87 (2.22)	17.86 (0.96)
Completeness (%)[a]	99.96 (100)	99.60 (98.67)
Multiplicity[a]	26.2 (27.6)	6.9 (6.8)
Refinement		
Resolution (Å)	2.98	2.65
No. reflections	87,496	58,703
R_{work}/R_{free}	0.204/0.231	0.248/0.264
Number of Atoms		
Protein	20,893	10,578
Nucleic acid	2,476	2,266
Ion/ligand	207	108
Water	52	30
B Factors		
Mean	85.59	107.88
Protein	87.55	106.31
Nucleic acid	68.43	116.48
Ion/ligand	98.52	89.65
Water	63.65	80.29
RMSDs		
Bond lengths (Å)	0.005	0.003
Bond angles (°)	0.68	0.62
Ramachandran Plot		
Favored (%)	97.08	97.88
Allowed (%)	2.92	2.12
Outliers (%)	0.00	0.00
Molprobity		
Clashscore	7.14	8.42

WT, wild-type.[a]Values in parentheses denote highest resolution shell.

PAM-interacting residues Lys613 and Lys671 move by ~1 Å and ~2.5 Å, respectively, toward the PAM of the dsDNA target. The intact dsDNA-bound complex displays a similar narrowing of the PI domain but additionally adopts a slightly more open conformation of the bilobed scaffold (RMSD: 4.51 Å; Figure 2D), in which the RuvC and Nuc domains have moved away from the REC lobe to accommodate the target dsDNA. The observation that the conformation of the FnCas12a-crRNA-ssDNA structure is similar to that of the two dsDNA-bound structures corroborates biochemical experiments demonstrating that crRNA-TS hybridization alone is sufficient to allosterically activate FnCas12a. Collectively, the structural studies reveal that both ssDNA and dsDNA target binding results in the REC2 domain moving away from the NUC lobe, thus permitting substrate DNA access to the now exposed RuvC catalytic site.

PAM Recognition Facilitates Target dsDNA Unwinding

The observation that target ssDNA binding is sufficient for allosteric activation of Cas12a implies that neither PAM recognition nor NTS coordination is per se required for the allosteric activation of the RuvC nuclease domain. However, the presence of a PAM in dsDNA targets is essential both during *cis* cleavage of target dsDNA (Zetsche et al., 2015) and for dsDNA target-mediated *trans* cleavage (Chen et al., 2018). Using a previously described fluorophore-quencher (FQ) reporter assay (Chen et al., 2018), we investigated the PAM requirement for dsDNA-induced *trans* activation of FnCas12a (i.e., activation of non-target ssDNA cleavage in *trans*; Figure 2A). *Trans* activation of FnCas12a was highest in the presence of a single-stranded target DNA (TS), followed by dsDNA targets containing four (5′-TTTA-3′) or three (5′-TTA-3′) PAM base pairs (Figure 2B). dsDNA targets containing a 5′-CTA-3′ PAM also triggered *trans* activation of FnCas12a, albeit at a slightly lower efficiency. These observations are in agreement with a recent study reporting that FnCas12a efficiently targets DNA with 5′-YTA-3′ PAMs (Tu et al., 2017). In contrast, almost no *trans* cleavage was observed in the presence of dsDNA targets with shorter PAM motifs (Figure 2B). Similar results were observed for another set of dsDNA targets with different protospacer sequences (Figure S3). Thus, under the tested conditions, dsDNA-induced allosteric activation of Cas12a activity minimally required the presence of a 5′-YTV-3′ PAM.

Cas9 has been demonstrated to rely on PAM recognition to initiate unwinding of the protospacer segment in the dsDNA target, thus facilitating subsequent guide RNA invasion and R-loop formation (Anders et al., 2014; Jiang et al., 2016). As for Cas9, PAM recognition by FnCas12a induces a bend in the target DNA (Stella et al., 2017; Swarts et al., 2017), which could facilitate dsDNA unwinding and crRNA-TS hybridization. To test whether PAM binding is important for dsDNA unwinding in Cas12a, we extended our *trans* cleavage FQ-reporter assays to include DNA targets that had canonical (5′-TTTA-3′) or mutated (5′-GCGT-3′) PAM sequences and a 24-nt protospacer segment in which the TS and NTS were either fully duplexed (dsDNA) or unpaired (i.e., pre-unwound) within the protospacer (unwDNA) (Figure 2C). These experiments indicate that, although the presence of a PAM is required for *trans* activation by fully duplexed dsDNA targets, pre-unwound DNA targets induce *trans* cleavage activity in a PAM-independent manner. Similarly, the PAM was dispensable for *cis* cleavage of unwDNA (Figure 2D). It should be noted that, compared to canonical *cis* cleavage of

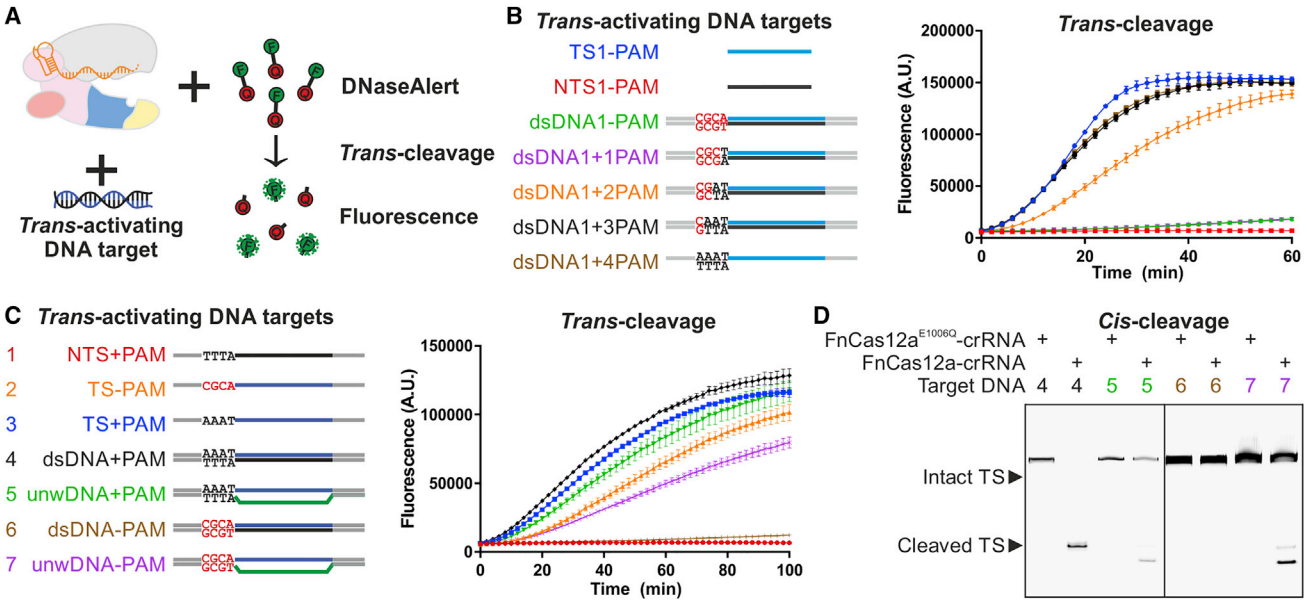


Figure 2. PAM Recognition Facilitates Target dsDNA Unwinding

(A) Schematic representation of the fluorophore-quencher (FQ) reporter-based *trans* cleavage experiment. DNA target binding by FnCas12a-crRNA complex triggers *trans* cleavage of non-target FQ reporter substrate; release of the fluorophore (F) results in increase of fluorescence signal.

(B) Target dsDNAs containing 5′-YTV-3′ PAMs trigger *trans* cleavage of a non-target FQ reporter. (Left) Schematic representation of ssDNA and dsDNA targets used in the experiments is shown. (Right) FnCas12a-crRNA complexes were incubated with ssDNA and dsDNA targets and a non-target FQ reporter. Fluorescence (A.U., arbitrary units) was measured over time. Data points represent the average of three replicates, and error bars indicate SD. For a FQ reporter-based experiment with *trans*-activating DNAs with another sequence, see Figure S3.

(C) The PAM is dispensable for *trans* cleavage of pre-unwound dsDNA targets. (Left) Schematic representation of ssDNA and dsDNA targets used in the experiments. (Right) Time-course analysis of FQ reporter cleavage by FnCas12a-crRNA in the presence of indicated ssDNA and dsDNA targets. Fluorescence (A.U., arbitrary units) was measured over time. Data points represent the average of three replicates, and error bars indicate SD.

(D) The PAM is dispensable for *cis* cleavage of pre-unwound dsDNA targets. Target DNA duplexes from (C), in which the TS 5′ end was labeled with Cy5, were incubated with FnCas12a-crRNA. Cleavage products were resolved by denaturing (7 M urea) PAGE.

dsDNA substrates, *cis* cleavage of unwDNA substrate was less efficient and yielded smaller TS cleavage products. This can possibly be explained by the fact that the protospacer is unpaired beyond the predicted cleavage location in the TS in the pre-unwound substrate (Stella et al., 2017; Zetsche et al., 2015), which could perturb the binding of the TS in the RuvC catalytic site and result in cleavage at a distinct site within the TS. Nevertheless, these findings corroborate observations that PAM binding is dispensable for allosteric activation of *trans*-nuclease activity in Cas12a. Collectively, these results thus suggest that PAM binding is required for strand separation in dsDNA target and progressive crRNA-TS hybridization, which results in subsequent allosteric activation of Cas12a.

Surface Electrostatics of the REC Lobe Orchestrates NTS Cleavage

Previously determined structures of FnCas12a bound to dsDNA targets in pre-cleavage (PDB: 5NFV) and post-cleavage (PDB: 5MGA) states revealed that guide crRNA-TS hybridization displaces 20 nt in the NTS (Stella et al., 2017; Swarts et al., 2017). As the displaced segment of the NTS contains the cleavage site, crRNA-TS hybridization would thus make the NTS susceptible to the ssDNase activity of the RuvC domain. However, there is currently little insight into the mechanism coupling crRNA-TS DNA hybridization to NTS DNA cleavage because an extensive portion of the NTS is structurally disordered in these complexes. To shed light on the mechanism of crRNA-guided target DNA cleavage, we determined an additional structure of a ternary complex comprising wild-type FnCas12a, a 43-nt crRNA, and a target dsDNA comprising full-length target and non-target strands. Although the complex contains the same dsDNA as our previously reported pre-cleavage structure (PDB: 5NFV), the new crystal structure, determined at a resolution of 2.65 Å, has significantly different unit cell dimensions (Table 1), indicative of a slightly different conformational state, which nevertheless corresponds to that of the pre-cleavage complex (PDB: 5NFV; RMSD 1.25 Å). The structure contains a near-complete R-loop in which NTS nucleotides 1–13, 19 and 20 are ordered (Figures 3A and 3B). NTS nucleotides 7–13 are bound in a positively charged groove on the outer surface of the RuvC domain by electrostatic contacts with Asn1288 and basic residues, including Lys895, Arg1014, Lys1066, Lys1069, Lys1281, and Lys1287 (Figures 3C and S4).

To test the importance of the NTS-binding groove residues for target cleavage, we substituted selected amino acid residues in the groove with alanine and generated the mutant proteins FnCas12a$^{R1014A\text{-}R1016A\text{-}K1066A\text{-}K1069A}$ and FnCas12a$^{K1281A\text{-}K1287A\text{-}N1288A}$. The *cis* cleavage efficiency of

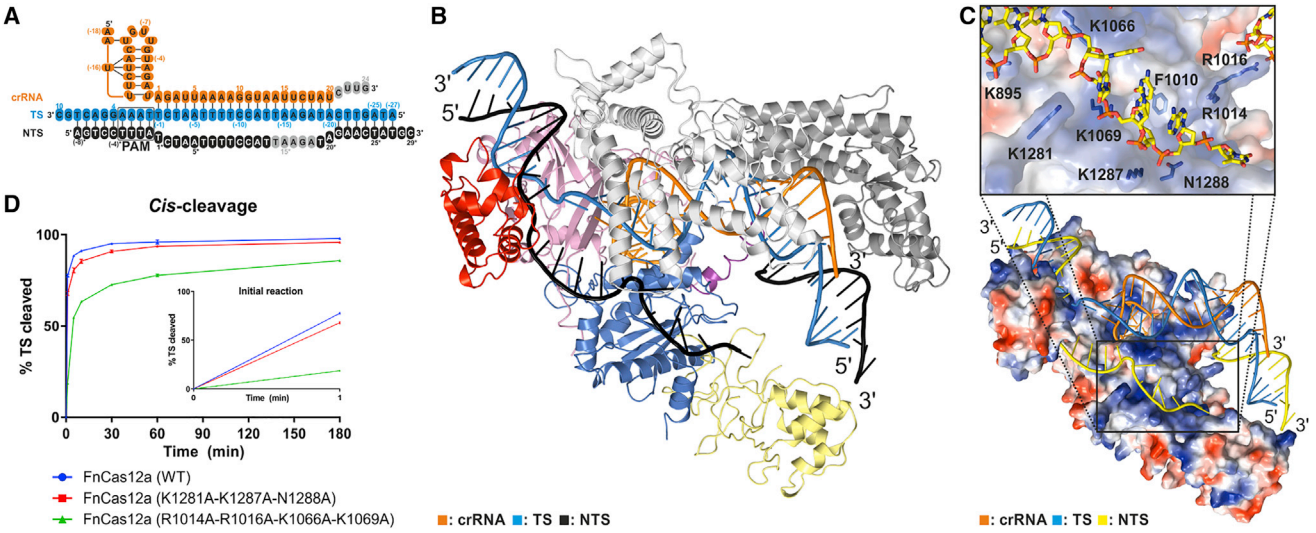


Figure 3. Surface Electrostatics of the REC Lobe Guides NTS Cleavage

(A) Sequences of the crRNA guide and TS and NTS DNA (see also Table S1) in the structure of the FnCas12a-crRNA-dsDNA complex. Structurally disordered nucleotides are colored gray.

(B) Overall structure of the FnCas12a-crRNA-dsDNA complex. Protein domains are colored according to the scheme in Figure 1B; nucleic acids are colored according to the scheme in (A). For details of FnCas12a-crRNA-TS binding interactions, see Figure S4.

(C) Surface electrostatic potential map of the FnCas12a NUC lobe reveals the NTS-binding groove. The NTS is colored yellow, and the REC lobe is omitted for clarity. Blue, positively charged region; red, negatively charged region. The inset panel displays the positively charged residues involved in NTS coordination. For a sequence alignment displaying the conservation of NTS residues, see Figure S5A. For structural conservation of the NTS-binding groove, see Figure S5B.

(D) Mutation of NTS-binding groove residues lowers *cis* cleavage efficiencies. FnCas12a, FnCas12a$^{K1218A-K1287A-K1288}$, and FnCas12a$^{R1014A-R016A-K1066A-K1069A}$ were incubated with a crRNA and a target dsDNA in which the TS was labeled with 5′-Cy5. Cleavage products were resolved by denaturing (7 M urea) PAGE. Data points represent the average of duplicates, and error bars indicate SD. The inset shows initial reaction curves.

FnCas12a$^{K1281A-K1287A-N1288A}$ was only slightly perturbed; FnCas12a$^{R1014A-R1016A-K1066A-K1069A}$ in turn showed greatly reduced *cis* cleavage activity (Figure 3D). This suggests that the NTS-binding groove contributes to energetic stabilization of the displaced NTS in the context of the R-loop, thereby promoting crRNA-TS DNA hybridization. Additionally, the NTS-binding groove provides a positively charged conduit connecting the PI domain and the RuvC active site and thus likely positions the NTS for insertion into the RuvC catalytic site (Figure 3C). The positively charged residues involved in NTS binding are partially conserved across the Cas12a nuclease family, and the positively charged NTS-binding groove is a prominent feature in other Cas12a orthologs (Figure S5).

Non-target DNA Strand Cleavage Precedes Target DNA Strand Cleavage

In our previous study, we provided evidence suggesting that Cas12 family enzymes generate double-strand DNA breaks by sequential cleavage of the two substrate DNA strands (Swarts et al., 2017). Based on the observation that the NTS-binding groove in FnCas12a appears to guide the displaced NTS into the RuvC catalytic site (Figure 3C), we hypothesized that the NTS is cleaved before the TS during dsDNA cleavage. To test this, we designed modified target dsDNA substrates in which either the TS or the NTS contained multiple backbone phosphorothioate modifications (Figure 4A). Such modifications typically inhibit cleavage by divalent cation-dependent nucleases (Eckstein and Gish, 1989). The phosphorothioate modifications did not affect FnCas12a-crRNA binding to the dsDNA targets because FnCas12a^{E1006Q}-crRNA bound both TS-modified and NTS-modified dsDNA targets as efficiently as unmodified control DNAs (Figure S6). Upon incubation with a catalytically active FnCas12a-crRNA complex, we observed that phosphorothioate modification of the TS did not affect *cis* cleavage of the NTS (Figure 4B). This indicates that NTS cleavage can occur independently of TS cleavage. In contrast, *cis* cleavage of the TS was almost completely abrogated in the dsDNA substrate in which the NTS was modified (Figure 4B), which suggests that the cleavage of the NTS is prerequisite for TS cleavage. To verify this, we tested dsDNA targets in which the phosphorothioate-modified NTS was either truncated, nicked, or contained a single unmodified "cleavable" phosphate (Figure 4C). TS cleavage occurred with all of the additional substrates. Of note, when the modified NTS was nicked, the TS was cleaved as efficiently as in the non-modified dsDNA target. Although we cannot rule out the possibility that the presence of the phophorothioate modifications in the NTS perturbs TS binding in the RuvC active site, this result strongly suggests that the phosphorothioate modifications in the NTS do not interfere with TS cleavage per se and implies that the NTS has to be cleaved before TS cleavage can occur.

One possible explanation for the sequentially ordered NTS and TS cleavage events is that the presence of an intact NTS in a dsDNA substrate sterically hinders the binding of the TS in the RuvC catalytic site. Alternatively, NTS cleavage might be

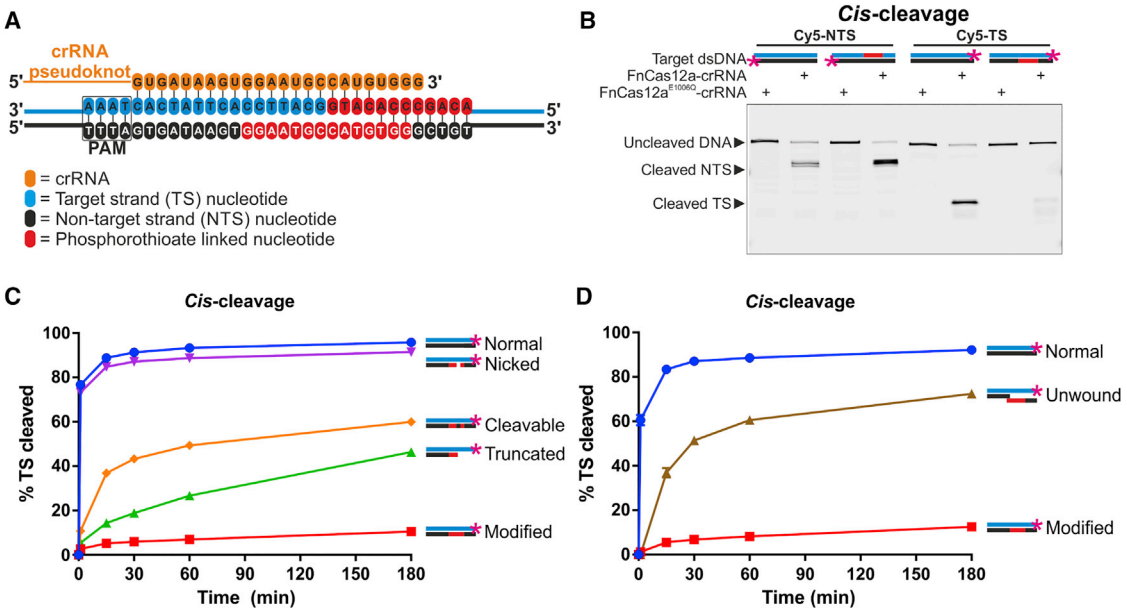


Figure 4. Non-target DNA Strand Cleavage Precedes Target DNA Strand Cleavage

(A) Schematic representation of the sequences of TS and NTS DNA used for the experiments in (B)–(D). Nucleotides colored red indicate nucleotides that are linked by phosphorothioates in modified TS and NTS strands. For electromobility shift assays that demonstrate that phosphorothioate modifications do not affect binding by FnCas12a-crRNA complexes, see Figure S6.

(B) FnCas12a cleaves the NTS and TS sequentially. Duplex DNA substrates in which one strand was modified and the other labeled with 5′-Cy5 were incubated with FnCas12a-crRNA, and cleavage products were resolved by denaturing (7 M urea) PAGE and visualized by fluorescence.

(C) Time-course analysis of cleavage of target DNA duplexes comprising modified NTS (as indicated) and 5′-Cy5-labeled TS. Data points in (C) represent the average of duplicates, and error bars indicate SD.

(D) FnCas12a cleaves the TS in a pre-unwound dsDNA target, even if the NTS carries non-cleavable phosphorothioate modifications. Time-course analysis of cleavage of target DNA duplexes comprising indicated NTS (unmodified, phosphorothioate-modified or pre-unwound by introducing mismatches between the TS and NTS) and 5′-Cy5-labeled TS. Data points represent the average of duplicates, and error bars indicate SD.

required for the unwinding of the PAM-distal dsDNA segment, which has to occur before the TS can enter the catalytic site. To investigate whether PAM-distal DNA unwinding affects TS cleavage, we tested whether partially unwound dsDNA targets could be cleaved regardless of NTS modifications. FnCas12a cleaved the TS in the unwound dsDNA target, albeit at lower efficiencies than for the unmodified dsDNA target (Figure 4D). Based on this result, we conclude that NTS cleavage enables local unwinding of the PAM-distal DNA duplex by fraying (Andreatta et al., 2006), which makes the TS susceptible for cleavage. Together, these observations imply that *cis* cleavage of dsDNA targets occurs in an ordered sequential manner in which the displaced NTS is cleaved first and the TS second.

Cas12a Releases the PAM-Distal End of Cleaved Target dsDNA

Studies of Cas9 previously revealed that dissociation of cleaved dsDNA targets from the Cas9-guide RNA complex is very slow (Richardson et al., 2016; Sternberg et al., 2014). This is likely a consequence of extensive interactions with both the PAM-proximal and PAM-distal ends of the cleaved dsDNA target. Unlike Cas9, Cas12a cleaves its target DNA distal from the PAM. Consequently, Cas12a engages in very few interactions with the PAM-distal cleavage product of a target dsDNA. To determine the fate of target DNA after Cas12a-mediated cleavage, we utilized dsDNA targets in which one of the four termini (i.e., either the 5′-TS, 3′-TS, 5′-NTS, or 3′-NTS) was labeled with a covalently attached fluorophore. All four target DNAs were efficiently bound by the catalytically inactive FnCas12a$^{E1006Q-R1218A}$-crRNA complex, as judged by fluorescence-detection size-exclusion chromatography (Figure S7). Upon incubation with a catalytically active FnCas12a-crRNA complex, the target DNAs were cleaved (Figure 5). The PAM-proximal cleavage product (i.e., 3′-TS and 5′-NTS-labeled DNAs) eluted together with the FnCas12a-crRNA complex, indicating that the PAM-proximal DNA remains bound to FnCas12a after cleavage. In contrast, the PAM-distal cleavage product (i.e., 5′-TS- and 3′-NTS-labeled DNAs) did not co-elute with the FnCas12a-crRNA complex, indicating that the PAM-distal DNA is released from the FnCas12a-crRNA complex upon cleavage. These findings are in agreement with recent single-molecule biophysical studies (Singh et al., 2018).

We further hypothesized that release of cleaved target DNA is required to clear the RuvC catalytic site and to allow subsequent *trans* cleavage of non-target DNA. To test this, we tested the *trans*-nuclease activity of FnCas12a-crRNA complexes incubated with dsDNA targets containing phosphorothioate modifications that prevent *cis* cleavage (Figure 5E) and thus consequently preclude release of the PAM-distal cleavage product. Although dsDNA targets carrying phosphorothioate

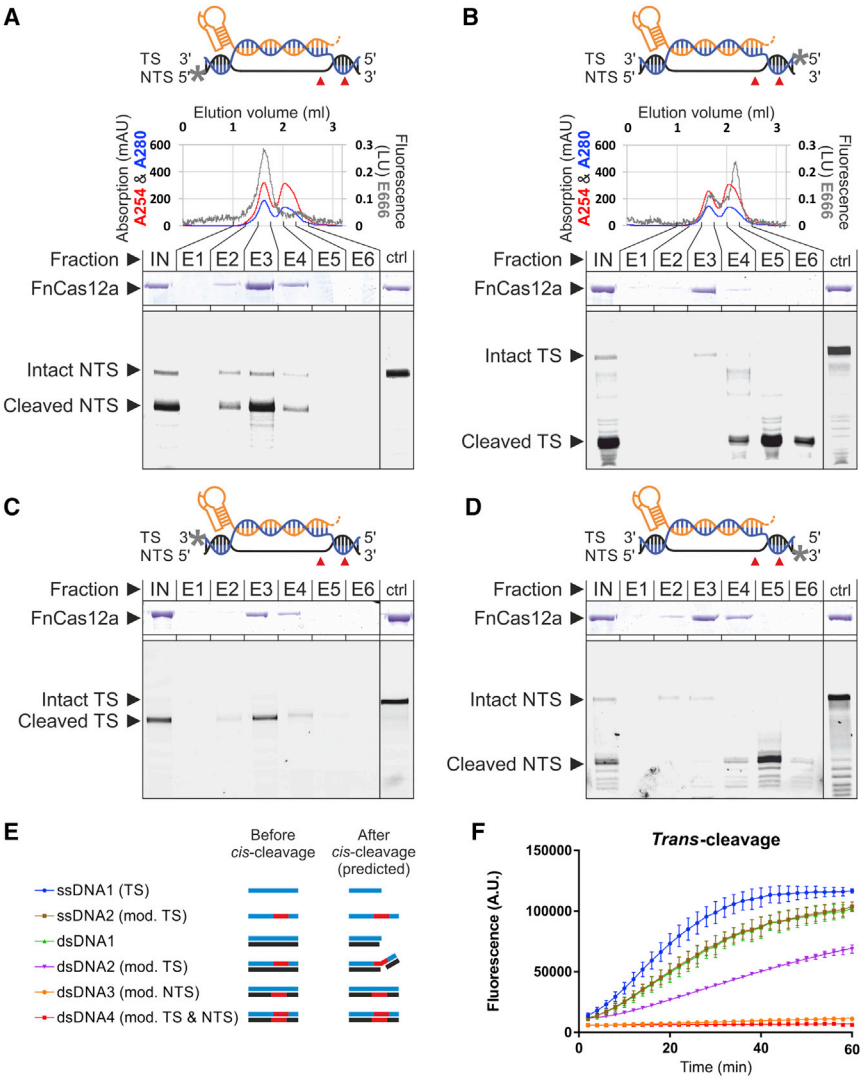


Figure 5. Cas12a-crRNA Releases the PAM-Distal Cleavage Product and Remains Bound to the PAM-Proximal Cleavage Product

(A–D) Fluorophore-labeled dsDNA targets were incubated with the FnCas12a-crRNA complex and analyzed by fluorescence-detection size-exclusion chromatography. Elution fractions were further analyzed for protein and fluorophore-labeled nucleic acid content by SDS-PAGE and denaturing (7 M urea) PAGE, respectively. In the schematic representation of the nucleic acids (top of each panel), the gray asterisk indicates the position of the fluorophore label and the red triangles indicate predicted TS (blue) and NTS (black) cleavage sites. ctrl, control sample containing catalytic mutant FnCas12a$^{E1006Q-R1218A}$ instead of FnCas12a; E1-6, elution fractions; IN, HPLC input. All HPLC chromatograms, including controls, are shown in Figure S7.

(E) Schematic representation of ssDNA and dsDNA targets used in the experiments and the (predicted) *cis* cleavage products of these targets that remain bound to FnCas12a.

(F) Release of the PAM-distal segment of the *cis* cleaved DNA targets facilitates *trans* cleavage of non-target DNA. FnCas12a-crRNA complexes were incubated with ssDNA and dsDNA targets and a non-target FQ-reporter. Fluorescence (A.U., arbitrary units) was measured over time. Data points represent the average of three replicates, and error bars indicate SD.

modifications are efficiently bound by FnCas12a (Figure S6), *trans* activation of FnCas12a by these targets was impaired compared to (unmodified) control ssDNA and dsDNA targets (Figure 5F); the TS-modified dsDNA target yielded reduced *trans* activation and the NTS-modified dsDNA target was incapable of *trans* activation. These results indicate that *cis* cleavage of dsDNA targets is required for dsDNA-induced *trans*-nuclease activity and imply that dissociation of the PAM-distal end of the dsDNA target is prerequisite for *trans* cleavage of non-target DNA.

DISCUSSION

Cas12-family enzymes exhibit two DNase activity modes; besides crRNA-guided *cis* cleavage of cDNA targets, these nucleases also catalyze *trans* cleavage of non-target ssDNA substrates upon binding and allosteric activation by a cDNA target (Chen et al., 2018; Li et al., 2018). The target DNA-induced, *trans*-acting DNase activity has been exploited to develop sensitive technologies for nucleic acid detection (Chen et al., 2018; Gootenberg et al., 2018). By combining insights into the *cis*- and *trans*-acting DNase activities derived from two FnCas12a-crRNA-DNA structures and biochemical experiments described here with insights from three recent complementary studies (Jeon et al., 2018; Singh et al., 2018; Strohkendl et al., 2018), we provide a revised mechanistic model for both *cis*- and *trans*-acting DNase activities of Cas12a enzymes (Figure 6).

Target dsDNA binding is initiated by recognition of the PAM sequence. In line with recent single-molecule biophysical studies (Jeon et al., 2018), our biochemical experiments show that the PAM is dispensable for cleavage of pre-unwound dsDNA targets, indicating that PAM recognition is mechanistically required for strand invasion of the crRNA in the target dsDNA and R-loop formation. A conserved lysine residue is inserted into the dsDNA duplex, possibly initiating TS-NTS unwinding (Swarts et al., 2017). PAM binding additionally introduces a kink in the TS, which further contributes to local strand separation and facilitates base pairing of the TS to the seed segment of the crRNA, and the displaced NTS is stabilized by interactions with the PI domain (Stella et al., 2017; Swarts et al., 2017). Progressive target DNA duplex unwinding is concomitant with crRNA-TS hybridization (Jeon et al., 2018; Singh et al., 2018; Strohkendl et al., 2018), which results in catalytic activation of Cas12a

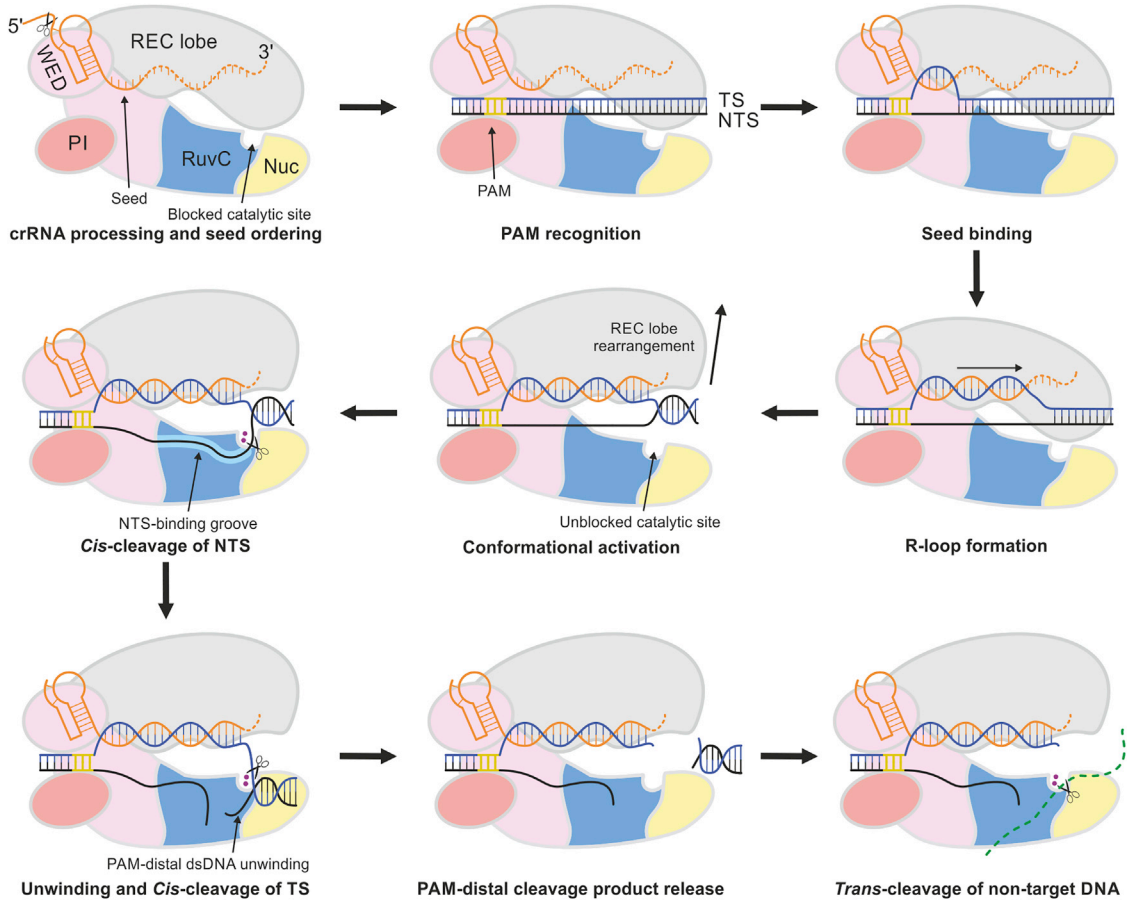


Figure 6. Schematic Model of Cas12a-Mediated *cis* and *trans* Cleavage of DNA

Cas12a processes the 5′ end of its own crRNA guide and pre-orders nucleotides 1–5 of the crRNA seed segment. Canonical dsDNA target recognition initiates with PAM recognition by the WED and PI domains, which promotes dsDNA target unwinding. R-loop formation is initiated by the TS binding the pre-ordered crRNA seed segment. Processive crRNA-TS hybridization and simultaneous TS-NTS unwinding result in the formation of the complete R-loop. crRNA-TS DNA hybirdization induces conformational changes in the REC lobe, resulting in allosteric unblocking of the catalytic site in the RuvC domain. The NTS binding groove guides the displaced NTS toward the RuvC catalytic site, resulting in *cis* cleavage of the NTS. Subsequently, further unwinding of the PAM-distal TS-NTS duplex allows the TS to enter the RuvC catalytic site, resulting in *cis* cleavage of the TS. The PAM-distal dsDNA is released, and the PAM-proximal dsDNA remains bound to the Cas12a-crRNA complex. This maintains Cas12a in a catalytically activated conformation, which permits *trans* cleavage of non-target ssDNAs.

upon formation of a complete R-loop. We show that crRNA-TS DNA hybridization, and not PAM binding per se, drives the allosteric activation of Cas12a by displacing the REC2 domain, thereby exposing the RuvC catalytic site. These findings provide a mechanistic rationale for previous studies demonstrating that 3′ truncations of the crRNA resulted in complete loss of Cas12a activity (Kim et al., 2017; Zetsche et al., 2015).

Overall, the mechanisms underpinning PAM-dependent target DNA recognition and R-loop formation in Cas12a are strikingly similar to those in Cas9 (Anders et al., 2014; Jiang et al., 2015; Sternberg et al., 2015) and likely a result of convergent evolution, given that Cas9 and Cas12a enzymes have distinct evolutionary histories and consequently different molecular architectures (Shmakov et al., 2017). However, there are notable mechanistic differences between Cas9 and Cas12a besides distinct PAM requirements. In contrast to Cas12a, the PAM is essential for dsDNA target cleavage by Cas9, even if the DNA is pre-unwound (Jeon et al., 2018). Additionally, Cas12a has a lower intrinsic tolerance for crRNA-TS mismatches compared to Cas9 and, as a consequence, requires higher complementarity between the crRNA and the TS before it is catalytically activated (Strohkendl et al., 2018). Importantly, the mechanisms for DNA cleavage differ substantially between the two enzymes; Cas9 utilizes a HNH and a RuvC domain to cleave the TS and NTS, respectively (Gasiunas et al., 2012; Jinek et al., 2012), while Cas12a utilizes a single RuvC domain for *cis* cleavage of both target DNA strands as well as for *trans* cleavage of non-target DNA.

The structure of FnCas12a R-loop complex reported here reveals that the displaced NTS is coordinated and oriented toward the RuvC catalytic site not only by the PI domain residues identified in earlier studies (Stella et al., 2017; Swarts et al., 2017) but additionally by several positively charged amino acid residues in the RuvC domain that form a structurally conserved NTS-binding groove. This not only contributes to

R-loop formation but also primes NTS for cleavage in the RuvC active site. As a result, dsDNA cleavage proceeds through an ordered sequential mechanism in which NTS is cleaved first, followed by the NTS, as recently shown by other studies (Jeon et al., 2018; Strohkendl et al., 2018) and verified by our experiments utilizing non-cleavable dsDNA substrates. Initial occupation of the RuvC catalytic site by the NTS might preclude TS cleavage. However, our experiments show that, in the absence of TS-NTS base pairing in the PAM-distal part of the R-loop, the TS can be cleaved even if the NTS is uncleavable. This implies that NTS cleavage is required to facilitate DNA strand separation in the PAM-distal duplex, possibly by fraying of the cleaved NTS ends (Andreatta et al., 2006). Based on similarities with crystal structures of the related Cas12b nucleases (Yang et al., 2016), we speculate that the Nuc domain induces a kink in the TS upon binding, which promotes its insertion into the RuvC catalytic site and subsequent cleavage. Currently available crystal structures of Cas12a reveal substantial conformational flexibility of the Nuc domain with respect to the remainder of the NUC lobe, suggesting that the Nuc domain might play an active role in both unwinding and positioning of the TS. The unspecific ssDNase activity of the RuvC catalytic site of Cas12a can result in further trimming of the ends of the *cis*-cleaved target dsDNA, resulting in heterogeneous cleavage products. Similar observations have also been made for Cas9 (Stephenson et al., 2018), although Cas9 does not possess *trans*-nuclease activity. In contrast to Cas9, which contains two catalytic sites buried in its scaffold, Cas12a needs to have its single catalytic site solvent exposed to allow association first with the NTS and subsequently with the TS. We hypothesize that *trans* cleavage of non-target ssDNA might be a consequence of the evolutionary history of Cas12 nucleases that has been preserved due to the requirement to catalyze both TS and NTS cleavage using a single active site. Corroborating recent studies (Jeon et al., 2018; Singh et al., 2018; Strohkendl et al., 2018), we finally show that, upon sequential cleavage of the two DNA strands of a dsDNA target, the PAM-distal cleavage product is released, and the PAM-proximal cleavage product remains bound to Cas12a. This maintains Cas12a in a catalytically competent state, in which its RuvC active site remains exposed to solvent and is poised to catalyze *trans* cleavage of non-target ssDNA substrates. However, the exact mechanism by which ssDNA substrates bind in and are cleaved by the RuvC catalytic site remains to be determined.

The insights provided by this study likely apply to other Cas12a orthologs, as well as to Cas12b nucleases. Similar to Cas12a, Cas12b demonstrates *cis*- and *trans*-acting DNase activities (Chen et al., 2018). Moreover, the RuvC nuclease domain in Cas12b is responsible for cleavage of both the TS and NTS DNA strands in a dsDNA target (Liu et al., 2017; Yang et al., 2016). These findings are important in the context of the biological function of type V CRISPR-Cas systems in genome defense as it demonstrates that they can target both ssDNA and dsDNA invasive nucleic acid elements. Furthermore, following cleavage of an invading target dsDNA, the persistence of *trans*-acting DNase activity might contribute to the interference mechanism and invader clearance.

Finally, our mechanistic insights have implications for further development and utilization of Cas12a as a genome-editing tool. Cas12a orthologs, including FnCas12a, have successfully been used for genome editing in bacteria, yeast, insects, plants, and mammalian cells, including human cell lines (Swarts and Jinek, 2018). As Cas12a does not only cleave target genomic dsDNA in *cis* but also non-target ssDNA in *trans*, it could potentially target transcription or replication intermediates, or ssDNA templates that are used for homology-directed repair (Richardson et al., 2016). Although Cas12a has a low intrinsic tolerance for off-target cleavage (Strohkendl et al., 2018), the significance of non-target DNA *trans* cleavage by Cas12a for genome editing awaits further investigation. The NTS-binding groove might be an interesting target for structure-guided engineering of Cas12a to increase its specificity. It has previously been demonstrated that mutating residues involved in NTS coordination can lower mismatch tolerance in both Cas9 and Cas12a (Chen et al., 2017; Gao et al., 2017; Kleinstiver et al., 2016; Slaymaker et al., 2016). Additional mutations of NTS-binding residues could further enhance the specificity of Cas12a variants. Lastly, asymmetric retention and release of DSB ends upon Cas12a-catalyzed cleavage suggests that editing efficiency or DNA repair outcomes might be dependent on the orientation of the bound Cas12a, particularly in the context of multiplexed genome editing. In conclusion, our studies revealed critical insights into the molecular mechanisms of target DNA binding and both *cis* and *trans* cleavage of DNA substrates by type V CRISPR effector nucleases, providing a framework for their further development for genome-editing applications.

STAR★METHODS

Detailed methods are provided in the online version of this paper and include the following:

- KEY RESOURCES TABLE
- CONTACT FOR REAGENT AND RESOURCE SHARING
- EXPERIMENTAL MODEL AND SUBJECT DETAILS
  - *Escherichia coli* Rosetta (DE3)
- METHOD DETAILS
  - FnCas12a expression and purification
  - Crystallization and structure determination
  - Structure analysis
  - M13 DNA trans-cleavage experiments
  - FQ-reporter trans-cleavage assays
  - Cis-cleavage experiments
  - High-performance liquid chromatography experiments
- DATA AND SOFTWARE AVAILABILITY

SUPPLEMENTAL INFORMATION

Supplemental Information includes seven figures and two tables and can be found with this article online at https://doi.org/10.1016/j.molcel.2018.11.021.

ACKNOWLEDGMENTS

We are grateful to Meitian Wang, Vincent Olieric, and Takashi Tomizaki at the Swiss Light Source (Paul Scherrer Institute, Villigen, Switzerland) for assistance with X-ray diffraction measurements. We thank members of the Jinek

group for discussions and critical reading of the manuscript. This work was supported by Swiss National Science Foundation (SNSF) project grants to M.J. (SNSF 31003A_149393 and 31003A_182567) and by long-term postdoctoral fellowships from the European Molecular Biology Organization (EMBO) to D.C.S. (ALTF 179-2015 and aALTF 509-2017). M.J. is International Research Scholar of the Howard Hughes Medical Institute and Vallee Scholar of the Bert L & N Kuggie Vallee Foundation.

AUTHOR CONTRIBUTIONS

D.C.S. and M.J. designed experiments. D.C.S. prepared and crystallized the Cas12a complexes, collected X-ray data, determined crystal structures, and carried out biochemical assays. D.C.S. and M.J. wrote the manuscript.

DECLARATION OF INTERESTS

M.J. is a co-founder of Caribou Biosciences and member of its scientific advisory board.

Received: June 22, 2018
Revised: September 14, 2018
Accepted: November 15, 2018
Published: January 10, 2019

REFERENCES

Afonine, P.V., Grosse-Kunstleve, R.W., Echols, N., Headd, J.J., Moriarty, N.W., Mustyakimov, M., Terwilliger, T.C., Urzhumtsev, A., Zwart, P.H., and Adams, P.D. (2012). Towards automated crystallographic structure refinement with phenix.refine. Acta Crystallogr. D Biol. Crystallogr. *68*, 352–367.

Anders, C., Niewoehner, O., Duerst, A., and Jinek, M. (2014). Structural basis of PAM-dependent target DNA recognition by the Cas9 endonuclease. Nature *513*, 569–573.

Andreatta, D., Sen, S., Pérez Lustres, J.L., Kovalenko, S.A., Ernsting, N.P., Murphy, C.J., Coleman, R.S., and Berg, M.A. (2006). Ultrafast dynamics in DNA: "fraying" at the end of the helix. J. Am. Chem. Soc. *128*, 6885–6892.

Barrangou, R., and Doudna, J.A. (2016). Applications of CRISPR technologies in research and beyond. Nat. Biotechnol. *34*, 933–941.

Chen, J.S., Dagdas, Y.S., Kleinstiver, B.P., Welch, M.M., Sousa, A.A., Harrington, L.B., Sternberg, S.H., Joung, J.K., Yildiz, A., and Doudna, J.A. (2017). Enhanced proofreading governs CRISPR-Cas9 targeting accuracy. Nature *550*, 407–410.

Chen, J.S., Ma, E., Harrington, L.B., Da Costa, M., Tian, X., Palefsky, J.M., and Doudna, J.A. (2018). CRISPR-Cas12a target binding unleashes indiscriminate single-stranded DNase activity. Science *360*, 436–439.

Dong, D., Ren, K., Qiu, X., Zheng, J., Guo, M., Guan, X., Liu, H., Li, N., Zhang, B., Yang, D., et al. (2016). The crystal structure of Cpf1 in complex with CRISPR RNA. Nature *532*, 522–526.

Eckstein, F., and Gish, G. (1989). Phosphorothioates in molecular biology. Trends Biochem. Sci. *14*, 97–100.

Emsley, P., and Lohkamp, B. (2010). Features and development of Coot. Acta Crystallogr. D Biol. Crystallogr. *66*, 486–501.

Gao, P., Yang, H., Rajashankar, K.R., Huang, Z., and Patel, D.J. (2016). Type V CRISPR-Cas Cpf1 endonuclease employs a unique mechanism for crRNA-mediated target DNA recognition. Cell Res. *26*, 901–913.

Gao, L., Cox, D.B.T., Yan, W.X., Manteiga, J.C., Schneider, M.W., Yamano, T., Nishimasu, H., Nureki, O., Crosetto, N., and Zhang, F. (2017). Engineered Cpf1 variants with altered PAM specificities. Nat. Biotechnol. *35*, 789–792.

Gasiunas, G., Barrangou, R., Horvath, P., and Siksnys, V. (2012). Cas9-crRNA ribonucleoprotein complex mediates specific DNA cleavage for adaptive immunity in bacteria. Proc. Natl. Acad. Sci. USA *109*, E2579–E2586.

Gootenberg, J.S., Abudayyeh, O.O., Kellner, M.J., Joung, J., Collins, J.J., and Zhang, F. (2018). Multiplexed and portable nucleic acid detection platform with Cas13, Cas12a, and Csm6. Science *360*, 439–444.

Hayward, S., and Lee, R.A. (2002). Improvements in the analysis of domain motions in proteins from conformational change: DynDom version 1.50. J. Mol. Graph. Model. *21*, 181–183.

Jeon, Y., Choi, Y.H., Jang, Y., Yu, J., Goo, J., Lee, G., Jeong, Y.K., Lee, S.H., Kim, I.S., Kim, J.S., et al. (2018). Direct observation of DNA target searching and cleavage by CRISPR-Cas12a. Nat. Commun. *9*, 2777.

Jiang, F., Zhou, K., Ma, L., Gressel, S., and Doudna, J.A. (2015). Structural biology. A Cas9-guide RNA complex preorganized for target DNA recognition. Science *348*, 1477–1481.

Jiang, F., Taylor, D.W., Chen, J.S., Kornfeld, J.E., Zhou, K., Thompson, A.J., Nogales, E., and Doudna, J.A. (2016). Structures of a CRISPR-Cas9 R-loop complex primed for DNA cleavage. Science *351*, 867–871.

Jinek, M., Chylinski, K., Fonfara, I., Hauer, M., Doudna, J.A., and Charpentier, E. (2012). A programmable dual-RNA-guided DNA endonuclease in adaptive bacterial immunity. Science *337*, 816–821.

Kabsch, W. (2010). XDS. Acta Crystallogr. D Biol. Crystallogr. *66*, 125–132.

Kim, H.K., Song, M., Lee, J., Menon, A.V., Jung, S., Kang, Y.-M., Choi, J.W., Woo, E., Koh, H.C., Nam, J.-W., and Kim, H. (2017). In vivo high-throughput profiling of CRISPR-Cpf1 activity. Nat. Methods *14*, 153–159.

Kleinstiver, B.P., Pattanayak, V., Prew, M.S., Tsai, S.Q., Nguyen, N.T., Zheng, Z., and Joung, J.K. (2016). High-fidelity CRISPR-Cas9 nucleases with no detectable genome-wide off-target effects. Nature *529*, 490–495.

Koonin, E.V., Makarova, K.S., and Zhang, F. (2017). Diversity, classification and evolution of CRISPR-Cas systems. Curr. Opin. Microbiol. *37*, 67–78.

Krissinel, E., and Henrick, K. (2007). Inference of macromolecular assemblies from crystalline state. J. Mol. Biol. *372*, 774–797.

Larkin, M.A., Blackshields, G., Brown, N.P., Chenna, R., McGettigan, P.A., McWilliam, H., Valentin, F., Wallace, I.M., Wilm, A., Lopez, R., et al. (2007). Clustal W and Clustal X version 2.0. Bioinformatics *23*, 2947–2948.

Li, S.-Y., Cheng, Q.-X., Liu, J.-K., Nie, X.-Q., Zhao, G.-P., and Wang, J. (2018). CRISPR-Cas12a has both cis- and trans-cleavage activities on single-stranded DNA. Cell Res. *28*, 491–493.

Liu, L., Chen, P., Wang, M., Li, X., Wang, J., Yin, M., and Wang, Y. (2017). C2c1-sgRNA complex structure reveals RNA-guided DNA cleavage mechanism. Mol. Cell *65*, 310–322.

McCoy, A.J., Grosse-Kunstleve, R.W., Adams, P.D., Winn, M.D., Storoni, L.C., and Read, R.J. (2007). Phaser crystallographic software. J. Appl. Cryst. *40*, 658–674.

Mohanraju, P., Makarova, K.S., Zetsche, B., Zhang, F., Koonin, E.V., and van der Oost, J. (2016). Diverse evolutionary roots and mechanistic variations of the CRISPR-Cas systems. Science *353*, aad5147.

Nishimasu, H., Yamano, T., Gao, L., Zhang, F., Ishitani, R., and Nureki, O. (2017). Structural basis for the altered PAM recognition by engineered CRISPR-Cpf1. Mol. Cell *67*, 139–147.e2.

Richardson, C.D., Ray, G.J., DeWitt, M.A., Curie, G.L., and Corn, J.E. (2016). Enhancing homology-directed genome editing by catalytically active and inactive CRISPR-Cas9 using asymmetric donor DNA. Nat. Biotechnol. *34*, 339–344.

Robert, X., and Gouet, P. (2014). Deciphering key features in protein structures with the new ENDscript server. Nucleic Acids Res. *42*, W320–W324.

Shmakov, S., Smargon, A., Scott, D., Cox, D., Pyzocha, N., Yan, W., Abudayyeh, O.O., Gootenberg, J.S., Makarova, K.S., Wolf, Y.I., et al. (2017). Diversity and evolution of class 2 CRISPR-Cas systems. Nat. Rev. Microbiol. *15*, 169–182.

Singh, D., Mallon, J., Poddar, A., Wang, Y., Tippana, R., Yang, O., Bailey, S., and Ha, T. (2018). Real-time observation of DNA target interrogation and product release by the RNA-guided endonuclease CRISPR Cpf1 (Cas12a). Proc. Natl. Acad. Sci. USA *115*, 5444–5449.

Slaymaker, I.M., Gao, L., Zetsche, B., Scott, D.A., Yan, W.X., and Zhang, F. (2016). Rationally engineered Cas9 nucleases with improved specificity. Science *351*, 84–88.

Stella, S., Alcón, P., and Montoya, G. (2017). Structure of the Cpf1 endonuclease R-loop complex after target DNA cleavage. Nature *546*, 559–563.

Stephenson, A.A., Raper, A.T., and Suo, Z. (2018). Bidirectional degradation of DNA cleavage products catalyzed by CRISPR/Cas9. J. Am. Chem. Soc. *140*, 3743–3750.

Sternberg, S.H., Redding, S., Jinek, M., Greene, E.C., and Doudna, J.A. (2014). DNA interrogation by the CRISPR RNA-guided endonuclease Cas9. Nature *507*, 62–67.

Sternberg, S.H., LaFrance, B., Kaplan, M., and Doudna, J.A. (2015). Conformational control of DNA target cleavage by CRISPR-Cas9. Nature *527*, 110–113.

Strohkendl, I., Saifuddin, F.A., Rybarski, J.R., Finkelstein, I.J., and Russell, R. (2018). Kinetic basis for DNA target specificity of CRISPR-Cas12a. Mol. Cell *71*, 816–824.e3.

Sun, H., Li, F., Liu, J., Yang, F., Zeng, Z., Lv, X., Tu, M., Liu, Y., Ge, X., Liu, C., et al. (2018). A single multiplex crRNA array for FnCpf1-mediated human genome editing. Mol. Ther. *26*, 2070–2076.

Swarts, D.C., and Jinek, M. (2018). Cas9 versus Cas12a/Cpf1: structure-function comparisons and implications for genome editing. Wiley Interdiscip. Rev. RNA *9*, e1481.

Swarts, D.C., van der Oost, J., and Jinek, M. (2017). Structural basis for guide RNA processing and seed-dependent DNA targeting by CRISPR-Cas12a. Mol. Cell *66*, 221–233.e4.

Świat, M.A., Dashko, S., den Ridder, M., Wijsman, M., van der Oost, J., Daran, J.-M., and Daran-Lapujade, P. (2017). FnCpf1: a novel and efficient genome editing tool for Saccharomyces cerevisiae. Nucleic Acids Res. *45*, 12585–12598.

Terwilliger, T. (2004). Solve and resolve: automated structure solution, density modification and model building. J. Synchrotron Radiat. *11*, 49–52.

Terwilliger, T.C., Read, R.J., Adams, P.D., Brunger, A.T., Afonine, P.V., and Hung, L.W. (2013). Model morphing and sequence assignment after molecular replacement. Acta Crystallogr. D Biol. Crystallogr. *69*, 2244–2250.

Tu, M., Lin, L., Cheng, Y., He, X., Sun, H., Xie, H., Fu, J., Liu, C., Li, J., Chen, D., et al. (2017). A 'new lease of life': FnCpf1 possesses DNA cleavage activity for genome editing in human cells. Nucleic Acids Res. *45*, 11295–11304.

Wang, H., La Russa, M., and Qi, L.S. (2016). CRISPR/Cas9 in genome editing and beyond. Annu. Rev. Biochem. *85*, 227–264.

Wright, A.V., Nuñez, J.K., and Doudna, J.A. (2016). Biology and applications of CRISPR systems: harnessing nature's toolbox for genome engineering. Cell *164*, 29–44.

Yamano, T., Nishimasu, H., Zetsche, B., Hirano, H., Slaymaker, I.M., Li, Y., Fedorova, I., Nakane, T., Makarova, K.S., Koonin, E.V., et al. (2016). Crystal structure of Cpf1 in complex with guide RNA and target DNA. Cell *165*, 949–962.

Yamano, T., Zetsche, B., Ishitani, R., Zhang, F., Nishimasu, H., and Nureki, O. (2017). Structural basis for the canonical and non-canonical PAM recognition by CRISPR-Cpf1. Mol. Cell *67*, 633–645.e3.

Yang, H., Gao, P., Rajashankar, K.R., and Patel, D.J. (2016). PAM-dependent target DNA recognition and cleavage by C2c1 CRISPR-Cas endonuclease. Cell *167*, 1814–1828.e12.

Zetsche, B., Gootenberg, J.S., Abudayyeh, O.O., Slaymaker, I.M., Makarova, K.S., Essletzbichler, P., Volz, S.E., Joung, J., van der Oost, J., Regev, A., et al. (2015). Cpf1 is a single RNA-guided endonuclease of a class 2 CRISPR-Cas system. Cell *163*, 759–771.

STAR★METHODS

KEY RESOURCES TABLE

REAGENT or RESOURCE	SOURCE	IDENTIFIER
Chemicals, Peptides, and Recombinant Proteins		
Potassium chloride	Roth	6781.2
HEPES	Roth	HN78.1
Sodium citrate tribasic dihydrate	Fluka	71404
Magnesium chloride	Fluka	63064-500G
Potassium thiocyanate	Roth	P753.1
Bis-Tris propane	Sigma-Aldrich	B6755-250G
Poly(ethylene glycol) 3,350 –	Sigma-Aldrich	202444-500G
Ethylene Glycol	Fluka	03750
Proteinase K	ThermoFisher Scientific	EO0491
Ethylenediaminetetraacetic acid	Roth	8040.3
DNaseAlert	Integrated DNA Technologies	11-04-02-04
Deposited Data		
Atomic coordinates and structure factors	This study	PDB: 6I1K and 6I1L
Raw image data	This study	https://doi.org/10.17632/dvvxbf5v2p.1
Experimental Models: Organisms/Strains		
E. coli Rosetta (DE3)	Novagen	70954-3
Oligonucleotides		
List of oligonucleotides used in this study	This study	Table S1
Recombinant DNA		
List of plasmids used in this study	This study	Table S2
M13mp18 Single-stranded DNA	New England Biolabs	N4040S
M13mp18 RF I DNA	New England Biolabs	N4018S
Software and Algorithms		
XDS	Kabsch, 2010	http://xds.mpimf-heidelberg.mpg.de/
PHASER	McCoy et al., 2007	http://www.phaser.cimr.cam.ac.uk/index.php/Phaser_Crystallographic_Software
Coot	Emsley and Lohkamp, 2010	https://www2.mrc-lmb.cam.ac.uk/personal/pemsley/coot/
PHENIX	Afonine et al., 2012; Terwilliger 2004; Terwilliger et al., 2013	http://www.phenix-online.org/
PyMOL	The PyMOL Molecular Graphics System, Version 2.0 Schrödinger, LLC	https://www.pymol.org/
DynDom	Hayward and Lee, 2002	http://fizz.cmp.uea.ac.uk/dyndom/
PDBePISA	Krissinel and Henrick, 2007	http://www.ebi.ac.uk/pdbe/pisa/
Clustal Omega	Larkin et al., 2007	https://www.ebi.ac.uk/Tools/msa/clustalo/
ESPript 3.0	Robert and Gouet, 2014	http://espript.ibcp.fr
GraphPad Prism 6	GraphPad Prism 5 for Windows, Version 6.07	https://www.graphpad.com
ImageQuant TL	ImageQuant TL 1D version 8.1	https://www.gelifesciences.com

CONTACT FOR REAGENT AND RESOURCE SHARING

Further information and requests for resources and reagents should be directed to and will be fulfilled by the Lead Contact, Martin Jinek (jinek@bioc.uzh.ch).

EXPERIMENTAL MODEL AND SUBJECT DETAILS

Escherichia coli Rosetta (DE3)

For protein expression, *E. coli* Rosetta (DE3) was grown in LB at 37°C in a shaker incubator at 120 rpm until an $OD_{600\ nm}$ of 0.6 was reached after the temperature was switched to 20°C. After 30 min, expression was induced by addition of isopropyl-1-thio-β-D-galactopyranoside (IPTG) to a final concentration of 0.2 mM. Expression took place at 20°C for 16 h.

METHOD DETAILS

FnCas12a expression and purification

FnCas12a mutant expression vectors were generated by Gibson assembly using pDS015 as backbone vector, which was amplified using oligonucleotides oDS366 and oDS367 or oDS368 and oDS369. Inserts were generated by annealing two oligonucleotides (oDS364 and oDS365) or ordered as dsDNA gBlock (gbDS02). FnCas12a and FnCas12a mutants were expressed in *E. coli* Rosetta DE3 and purified as described previously (Swarts et al., 2017). A detailed step-by-step protocol can be found online at bio-protocol (https://bio-protocol.org/e2842).

Crystallization and structure determination

The ternary FnCas12a-crRNA-TS complex was reconstituted by combining purified apo-FnCas12a^{E1006Q} in SEC buffer (500 mM KCl, 20 mM HEPES-KOH (pH 7.5), 1 mM DTT) at a concentration of 10 mg.ml^{-1} with synthetic crRNA1 (obtained from Integrated DNA Technologies, Table S1) in a 1:1.4 molar ratio (FnCas12a:crRNA1) in the presence of 5 mM $MgCl_2$, and incubating for 10 min at RT. Next, the TS DNA oDS311 (Table S1) was added in a 1:1.4:1.6 ratio (FnCas12a:crRNA1:oDS311). The complex was crystallized at 20°C using the hanging drop vapor diffusion method by mixing equal volumes of protein and reservoir solution. Initial spherulites were obtained at a protein concentration of 8.3 mg.ml^{-1} with 1.6 M trisodium citrate as reservoir solution. Crystal growth was optimized by iterative microseeding. Data were collected from a crystal that was grown for four weeks at 20°C in a protein concentration of 8.3 mg.ml^{-1} and 1.6 M trisodium citrate as reservoir solution. Crystals were transferred to a cryoprotectant solution (1.44 M trisodium citrate, 10% (v/v) ethylene glycol) and flash-cooled in liquid nitrogen.

The ternary FnCas12a-crRNA-DNA complex was reconstituted and crystallized as described previously for the FnCas12a-crRNAX-DNA ternary complex (Swarts et al., 2017). Diffraction data were obtained using a crystal grown for four months at 20°C in refinement screens with a final protein concentration of 7.7 mg.ml^{-1} and a reservoir solution containing 0.1 M Bis-Tris Propane (BTP; pH 6.5), 0.2 M KSCN, and 17.5% (w/v) polyethylene glycol 3,400. Crystals were transferred to a cryoprotectant solution (0.1 M BTP (pH 6.5), 0.2 M KSCN, 20% (w/v) polyethylene glycol 3,400, 15% (v/v) ethylene glycol, and 5 mM $MgCl_2$) and flash-cooled in liquid nitrogen.

X-ray diffraction data were measured at beamline X06DA (PXIII) of the Swiss Light Source (Paul Scherrer Institute, Villigen, Switzerland). Data were indexed, integrated, and scaled using XDS. Crystals of the FnCas12a-crRNA-TS ternary complex diffracted to a resolution of 2.98 Å and belonged to space group $P2_12_12_1$, with two copies of the complex in the asymmetric unit. The structure of the FnCas12a-crRNA-TS complex was solved by molecular replacement in phenix.phaser using a modified FnCas12a-crRNAX-dsDNA (PDB: 5NFV) as search model. Phases obtained using the initial molecular replacement solution were improved by density modification using phenix.resolve (Terwilliger 2004) and phenix.morph_model (Terwilliger et al., 2013). The atomic model was built manually in Coot (Emsley and Lohkamp, 2010) and refined using phenix.refine (Afonine et al., 2012). The final binary complex model contains crRNA1 residues (−18)–(+21), target strand residues (−20)-(−1) and FnCas12a^{E1006Q} residues 1–1299, except for residues 550-553, 1009-1013, 1156-1162, and 1277-1279, which lack ordered electron density.

The crystal of the FnCas12a-crRNA-dsDNA ternary complex diffracted to a resolution of 2.65 Å and belonged to space group $P2_1$, with one copy per asymmetric unit. The structure was solved by molecular replacement in phenix.phaser using a modified FnCas12a-crRNAX-dsDNA (PDB: 5NFV) as search model. The atomic model was built manually in Coot and refined using phenix.refine. The final ternary complex model contains crRNA residues (−18)–20, target DNA strand nucleotides (−27)–10, and non-target strand nucleotides (−8*)-13* and 19*-29*, and FnCas12a residues 1–1300, except for residues 850-851, 1135-1136, and 1153-1166, which lack ordered electron density.

Structure analysis

Root Means Square Deviations (RMSD) of structure alignments were calculated using Coot LSQ superpose in which main chain atoms were superposed (Emsley and Lohkamp, 2010). Domain movements were analyzed using DynDom (Hayward and Lee, 2002). Intramolecular interactions were analyzed using PDBePISA (Krissinel and Henrick, 2007). Vector maps were generated using the PyMol script Modevectors.

M13 DNA trans-cleavage experiments

To generate dsDNA targets, TS and NTS oligonucleotides (100 μM, oDS329-oDS342, Table S1) were mixed in a 1:4 molar ratio (TS:NTS). The strands were annealed by incubation at 95°C for 5 min, followed by slow cooling to room temperature. The samples were further diluted in H_2O to a concentration of 10 μM. For *trans*-cleavage experiments, FnCas12a and FnCas12^{E1006Q} (10 μM in

SEC buffer) were mixed with crRNA1 (10 μM in H_2O) in the presence of 5 mM $MgCl_2$ and incubated at 37°C for 10 min to allow binary complex formation. Target ssDNAs oDS302 or oDS311 (Table S1, 10 μM in H_2O) or target dsDNAs (10 μM in H_2O) and M13 circular ssDNA or dsDNA substrates (Table S2, 100 ng.μl^{-1}, New England Biolabs) were added. The final reaction (20 μl) contained final concentrations of 0.5x SEC buffer, 2.5 μM FnCas12a or FnCas12a^{E1006Q}, 1.5 μM crRNA1, 5 mM $MgCl_2$, 1.5 μM *trans*-activating ssDNA or dsDNA, and 10 ng.μl^{-1} circular DNA substrate. Samples were incubated for 90 min at 37°C. Reactions were stopped by adding EDTA and Proteinase K (Thermo Fisher Scientific) to final concentrations of 80 mM and 0.8 mg.ml^{-1}, respectively, and incubating for 30 min at 37°C. *Trans*-activating dsDNA was removed from the M13 circular ssDNA using the NucleoSpin® Gel and PCR Clean-up kit (MACHERY-NAGEL) according to the instructions of the manufacturer, with 7-fold excess of NTI DNA binding buffer. 6x DNA loading dye (Thermo Fisher Scientific) was added to the sample and the DNA was resolved on 0.8% (w/v) agarose gels stained with GelRed Nucleic Acid Gel Stain (Biotum) and visualized using a ChemiDoc Touch gel imager (Bio-Rad).

FQ-reporter trans-cleavage assays

To generate dsDNA targets, TS and NTS oligonucleotides (100 μM in H_2O; Table S1) were mixed (Table S2) in a 1:49 ratio (final target concentration: 2 μM). The strands were annealed by incubation at 95°C for 5 min, followed by slow cooling to room temperature. For *trans*-cleavage activity assays, FnCas12a was mixed with crRNA1 (10 μM in H_2O) or crRNA-λ (10 μM in H_2O) in the presence of 10 mM $MgCl_2$ and incubated at 37°C for 10 min to allow binary complex formation. The sample was diluted 10-fold in dilution buffer (0.5x SEC, 10 mM $MgCl_2$) and 2.5 μL target DNA was added to 50 μL of the protein sample. This sample was mixed with 47.5 μL DNaseAlert (IDT) solution (diluted in H_2O) in a 384-well plate. The final reaction (100 μl) contained final concentrations of 0.25x SEC buffer, 5 mM $MgCl_2$, 150 nM FnCas12a, 50 nM crRNA, 50 nM DNA *trans*-activating DNA target and 50 nM DNaseAlert substrate. Fluorescence signal (excitation at 536 nm, emission at 556 nm) was measured over time using a PHERAstar FSX (BMG Labtech) microplate reader with a FP 540-590-590 optical module. Experiments were performed in triplicates. Graphs (displaying averages and standard deviations for triplicates) were generated using GraphPad Prism 6.

Cis-cleavage experiments

The dsDNA targets with modified backbones used in the *cis*-cleavage experiments shown in Figure 4F were generated by mixing TS and NTS oligonucleotides (100 μM, Table S1) in a 1:2 ratio (unlabeled:Cy5-labeled). The strands were annealed by incubation at 95°C for 5 min, followed by slow cooling to room temperature. The samples were mixed in a 1:1 ratio with native loading dye (0.5x SEC buffer, 5 mM MgCl2, 50% (v/v) glycerol) and resolved on a 10% native polyacrylamide gel. Gel regions containing fluorophore-labeled dsDNA were identified using a Typhoon FLA 9500 gel imager (GE Healthcare) and cut out. The gel was crushed and soaked in H_2O for two days before the supernatant was extracted. The dsDNA was isolated from the supernatant by ethanol precipitation and dissolved in H_2O. The final concentration of the dsDNA targets was ~0.3 μM.

For all other *cis*-cleavage experiments, dsDNA targets were generated by mixing Cy5-labeled TS and NTS oligonucleotides (100 μM, Table S1) in a 1:4 ratio (TS-NTS). The strands were annealed by incubation at 95°C for 5 min, followed by slow cooling to room temperature. Samples were diluted to a final dsDNA concentration of 1 μM. FnCas12a or FnCas12a$^{E1006Q-R1218A}$ (10 μM in SEC buffer), crRNA-λ (10 μM), and $MgCl_2$ (50 mM) were mixed and incubated for 10 min at 37°C before the target dsDNA (0.3-1 μM) was added. The final 20 μL reaction contained final concentrations of 0.25x SEC buffer, 2.5 μM FnCas12a or FnCas12a$^{E1006Q-R1218A}$, 1 μM crRNA-λ, 2.5 mM $MgCl_2$, and 30-100 nM target dsDNA, and was incubated for 30 min at 20°C unless otherwise indicated. Reactions were stopped by adding EDTA and Proteinase K (Thermo Fisher Scientific) to final concentrations of 80 mM and 0.8 mg.ml^{-1}, respectively, and incubating for 30 min at 37°C. Samples were mixed 1:1 with 2x loading dye (5% glycerol (v/v), 90% formamide (v/v), and 2.5 mM EDTA), heated for 10 min at 95°C, and resolved on 20% denaturing (7 M Urea) polyacrylamide gels. Fluorescence of the Cy5-labeled DNA was detected using a Typhoon FLA 9500 gel imager (GE Healthcare). ImageQuant TL 1D (version 8.1) was used to analyze the fluorescence signal strength. Experiments were performed in duplicates. Graphs (displaying averages and standard deviations for duplicates) were generated using GraphPad Prism 6.

High-performance liquid chromatography experiments

Labeled and unlabeled target strand oligonucleotides (100 μM, Table S1) and labeled and unlabeled non-target strand oligonucleotides (100 μM, Table S1) were mixed in a 1:2 ratio (labeled:unlabeled) and annealed by incubation at 95°C for 5 min, followed by slow cooling to room temperature. The formed dsDNA targets were diluted in water to 10 μM. Prior to high-performance liquid chromatography (HPLC) analysis, FnCas12a or FnCas12a$^{E1006Q-R1218A}$, crRNA-λ (10 μM), $MgCl_2$ (50 mM), SEC buffer, and target DNA (10 μM) were mixed. The resulting 100 μL reaction contained final concentrations of 0.5x SEC buffer, 2 μM FnCas12a or FnCas12a$^{E1006Q-R1218A}$, 1 μM crRNA-λ, 2.5 mM $MgCl_2$, and 0.25 μM target dsDNA, and was incubated for 1 h at 37°C. Samples were resolved by HPLC on a Superdex 200 5/150 size exclusion column (GE Life Science) with a 3 mL bed volume and 20 bar pressure limit, which was equilibrated and run in 0.5x SEC at a flow rate of 0.1 ml.min^{-1}. Absorption at 280nm and 260nm and the fluorescent signal of Cy5- or ATTO532-labeled DNA were recorded throughout the run. For each

target dsDNA, fractions were collected and subsequently analyzed by SDS-PAGE for protein content and by 20% denaturing (7 M Urea) PAGE for DNA content. Fluorescence of the Cy5- or ATTO532-labeled DNA was detected using a Typhoon FLA 9500 gel imager (GE Healthcare).

DATA AND SOFTWARE AVAILABILITY

The atomic coordinates and structure factors reported in this paper are deposited in the Protein Data Bank (PDB). The accession numbers for the structures reported in this paper are PDB: 6I1L (FnCas12a-crRNA-TS-only complex) and PDB: 6I1K (FnCas12a-crRNA-TS-NTS complex). The unprocessed image files, image file analysis, and raw microplate reader data used to prepare the figures in this manuscript are deposited in Mendeley Data and are available at https://doi.org/10.17632/dvvxbf5v2p.1.

Molecular Cell, Volume *73*

Supplemental Information

Mechanistic Insights into the *cis*- and *trans*-Acting DNase Activities of Cas12a

Daan C. Swarts and Martin Jinek

SUPPLEMENTAL FIGURES AND TABLES

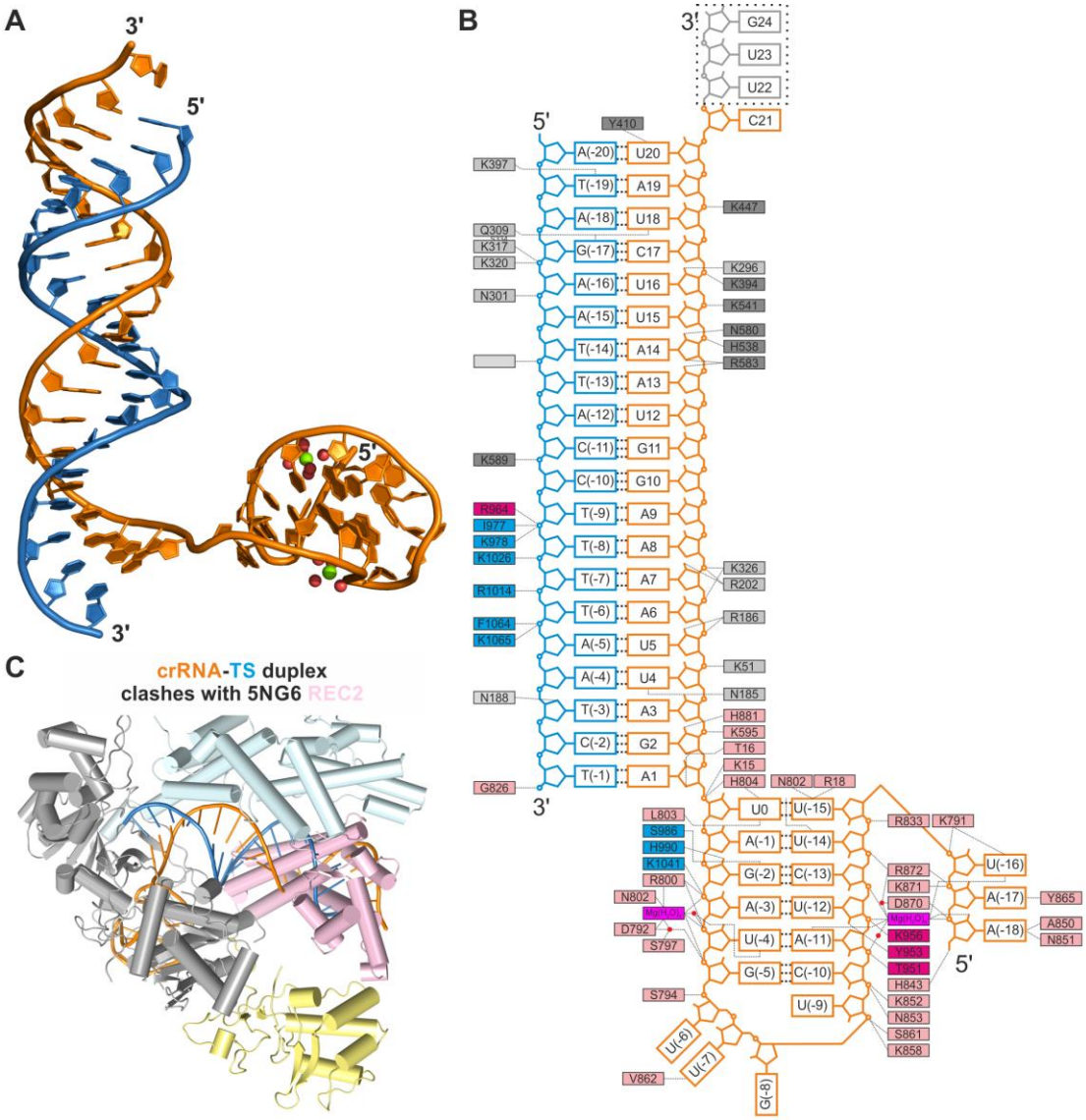


Figure S1. Details of FnCas12a-crRNA-ssDNA interactions. Related to Figure 1

(A) Structure of nucleic acids in the crystal structure of FnCas12a-crRNA complex bound to a target DNA strand. Water molecules are depicted as red spheres; Mg^{2+} ions are depicted as green spheres.

(B) Schematic representation of hydrogen bonding interactions between FnCas12a, nucleic acids, and divalent cations in the ternary structure. FnCas12a residues are colored according to their domains (see schematic representation in **Figure 1C**). Nucleotides colored grey are not ordered in the structure. Base pairs are indicated with thick dashed lines, while other hydrogen bonds are indicated with thin dashed lines. Red circles indicate water-mediated hydrogen bonding. Intra-crRNA pseudoknot hydrogen bonds in the crRNA are not displayed for clarity.

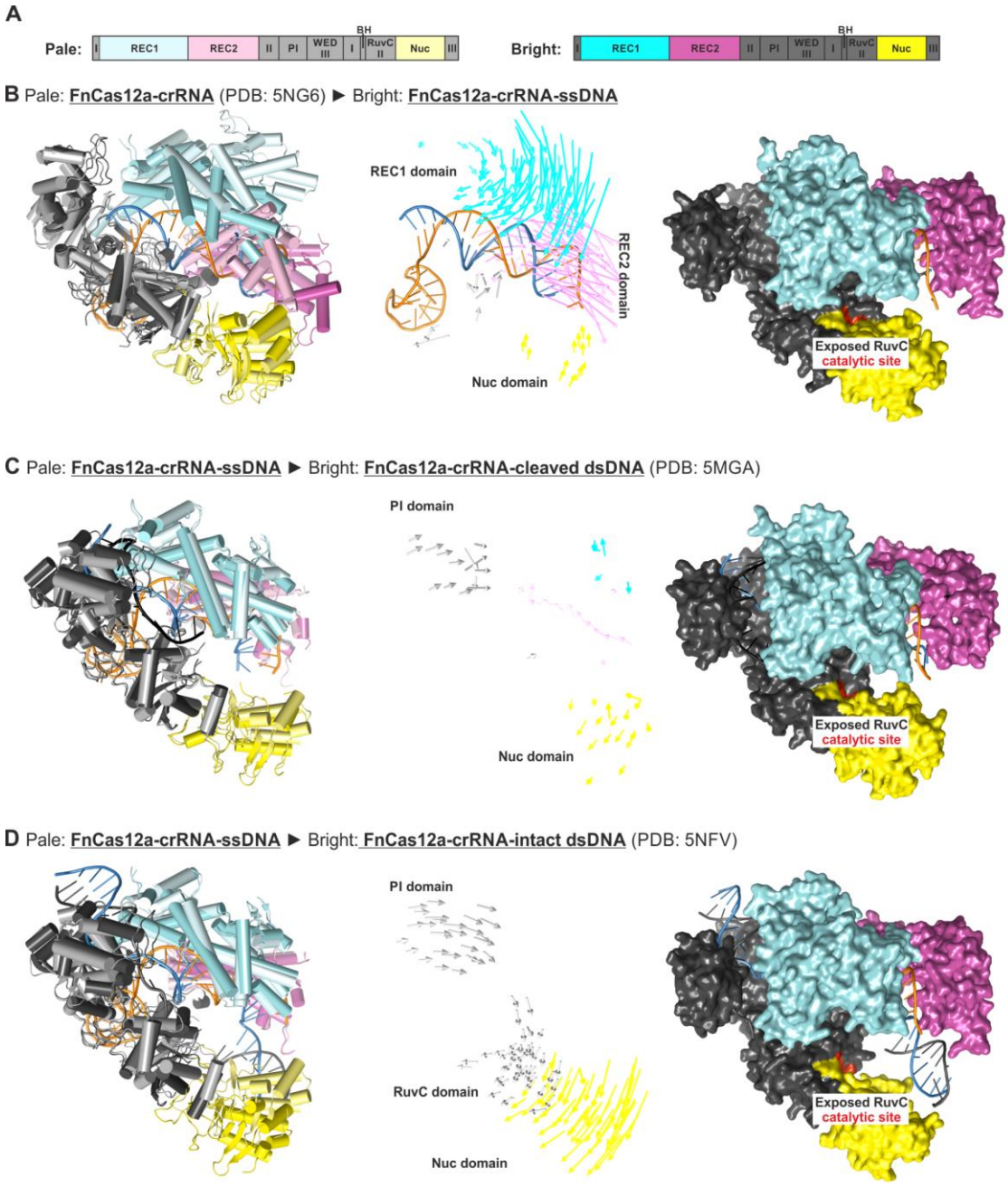


Figure S2. Conformational changes associated with allosteric activation of Cas12a. Related to Figure 1

(A) Schematic diagram of the domain organization of FnCas12a. REC, recognition; PI, protospacer adjacent motif (PAM) interacting; WED, wedge; BH, bridge helix; Nuc, nuclease. Both the WED and RuvC domains are formed by three discontinuous segments of the protein sequence. Pale and Bright coloring schemes correspond to different structures displayed in panels B-D.

(B-D) Comparison of structures of the binary FnCas12a-crRNA and ternary FnCas12a-crRNA-ssDNA complexes (panel B), ternary FnCas12a-crRNA-ssDNA and FnCas12a-crRNA-dsDNA (cleaved) complexes (panel C), and ternary FnCas12a-crRNA-ssDNA and FnCas12a-crRNA-dsDNA (intact) complexes (panel D). Left: superimposed structures. Domains are colored according to the scheme in panel A. Middle: Vector map displaying observed domain movement between two conformational states of FnCas12a. Vectors are colored according to the domain

color scheme indicated in panel A. Right: Surface representation of FnCas12a-crRNA in complex with a ssDNA target (panel B), intact dsDNA target (panel C), or cleaved dsDNA target (panel D) targets. Catalytic residues D917, E1006, and D1255 located in the RuvC domain are colored red.

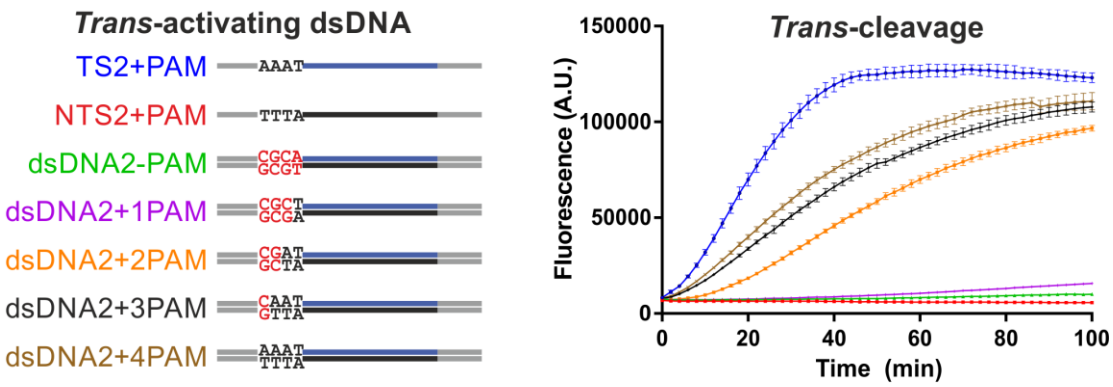


Figure S3. Target dsDNA containing a 5'-YTA-3' PAM trigger FnCas12a *trans*-cleavage of a non-target FQ-reporter. Related to Figure 2

Left: schematic representation of ssDNA and dsDNA targets used in the experiments. Right: FnCas12a-crRNA complexes were incubated with dsDNA targets and a non-target FQ-reporter. Fluorescence (A.U.: arbitrary units) was measured over time. Data points represent the average of three replicates and error bars indicate standard deviation. The crRNA and *trans*-activating DNAs in **Figure 2B** and **Figure S3** have different sequences.

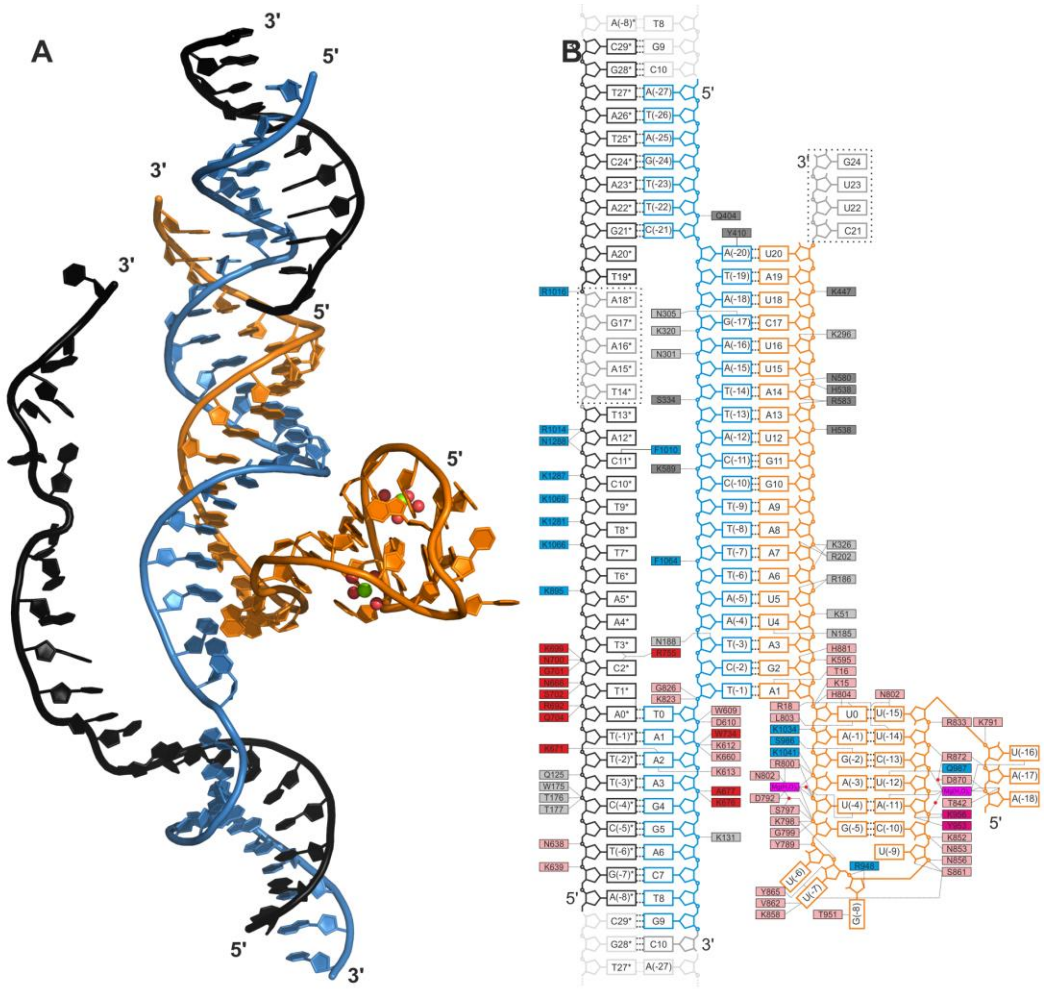


Figure S4. Details of FnCas12a-crRNA-dsDNA interactions. Related to Figure 3

(A) Structure of nucleic acids in the structure of FnCas12a-crRNA complex bound to a dsDNA target. Water molecules are depicted as red spheres; Mg^{2+} ions are depicted as green spheres.

(B) Schematic representation of hydrogen bonding interactions between FnCas12a, nucleic acids, and divalent cations in the ternary FnCas12a-crRNA-dsDNA structure. FnCas12a residues are colored according to their domains (see schematic representation in **Figure 1C**). Nucleotides colored grey are not ordered in the structure. Base pairs are indicated with thick dashed lines, while other hydrogen bonds are indicated with thin dashed lines. Red circles indicate water-mediated hydrogen bonding. Intra-crRNA pseudoknot hydrogen bonds in the crRNA are not displayed for clarity.

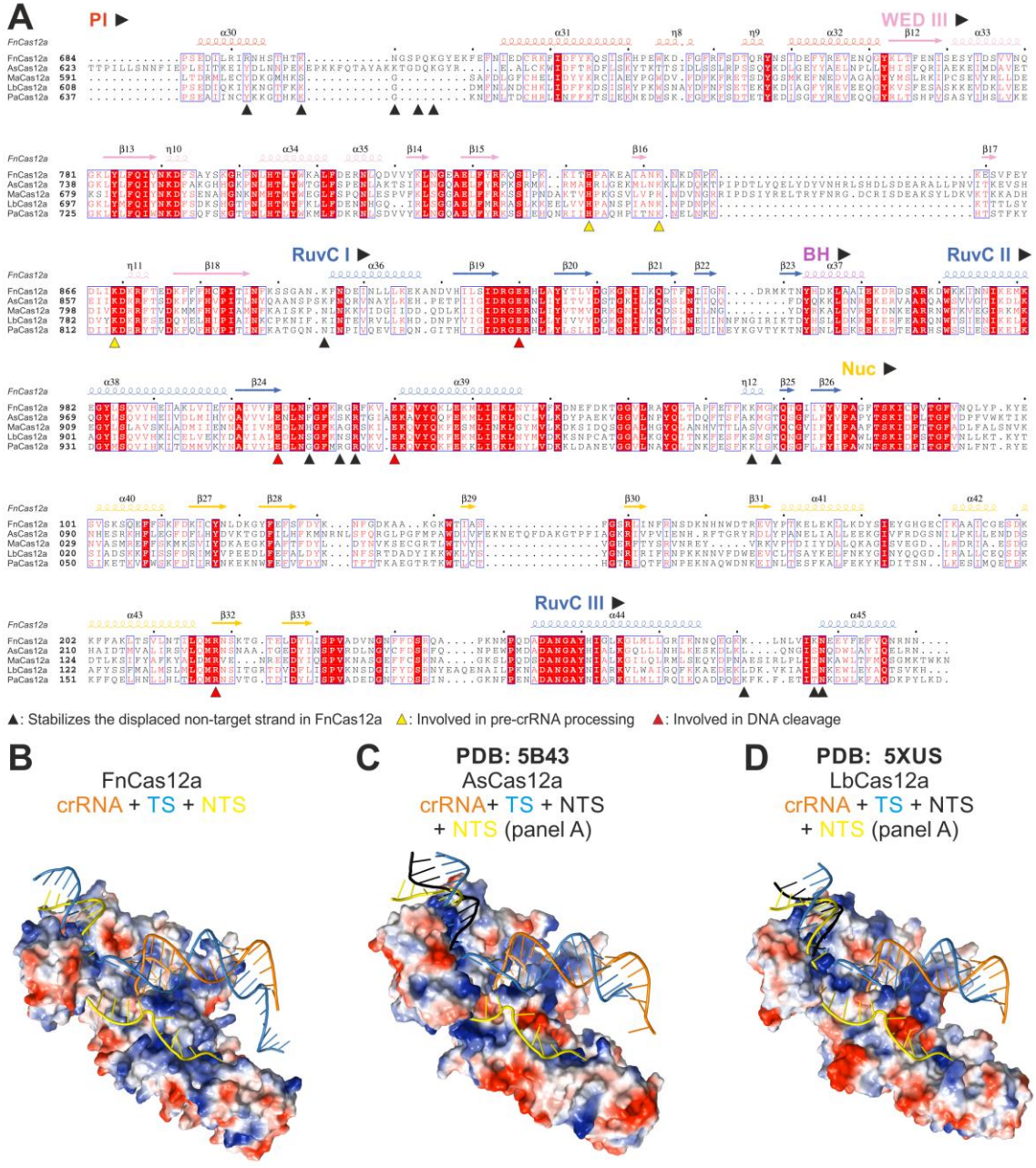


Figure S5. Conservation of the NTS-binding groove. Related to Figure 3

(A) Clustal Omega (Larkin et al., 2007) was used to generate a Multiple sequence alignment of Cas12a protein sequences of *Francisella novicida* U122 (FnCas12a), *Acidaminococcus sp.* BV3L6 (AsCas12a), *Methanomethylophilus alvus* Mx1201 (MaCas12a), and *Lachnospiraceae bacterium* ND2006 (LbCas12a). The Clustal Omega sequence alignment and the structural information from the structure of the binary FnCas12acrRNA complex were used as input for ESPript 3.0 (http://espript.ibcp.fr) (Robert and Gouet, 2014) to align secondary structure features to the sequence alignment. Residues important for specific FnCas12a functions are indicated with colored triangles.

(B) Surface electrostatic potential map of the NUC lobe of the FnCas12a-crRNA-dsDNA complex (as in Figure 4 panel C). The REC lobe is omitted for clarity. Blue, positively charged region; red, negatively charged region.

(C) Surface electrostatic potential map of the AsCas12a NUC lobe (PDB: 5B43). The REC lobe is omitted for clarity. The NTS (colored yellow) is modeled based on the structure of R-loop structure of the FnCas12a-crRNA-dsDNA complex. Blue, positively charged region; red, negatively charged region.

(D) Surface electrostatic potential map of the LbCas12a NUC lobe (PDB: 5XUS). The REC lobe is omitted for clarity. The NTS (colored yellow) is modeled based on the structure of R-loop structure of the FnCas12a-crRNA-dsDNA complex. Blue, positively charged surface; red, negatively charged surface.

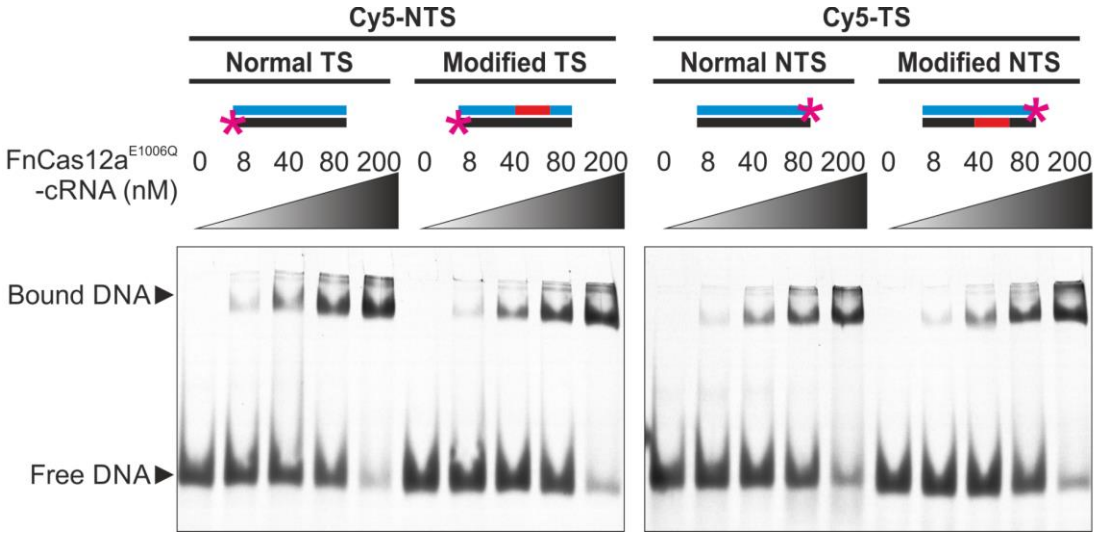


Figure S6. Phosphorothioate modification in the target and non-target DNA strands do not hamper binding by the FnCas12a-crRNA complex. Related to Figure 4

FnCas12a^{E1006Q}-crRNA complexes were incubated with dsDNA targets and complexes were resolved by native 8% polyacrylamide gel electrophoresis. Left: Electromobility Shift Assay using DNAs consisting of a Cy5-labeled NTS and normal or phosphorothioate-modified TS DNAs. Right: Electromobility Shift Assay using DNAs consisting of a Cy5-labeled TS and normal or phosphorothioate-modified NTS DNAs.

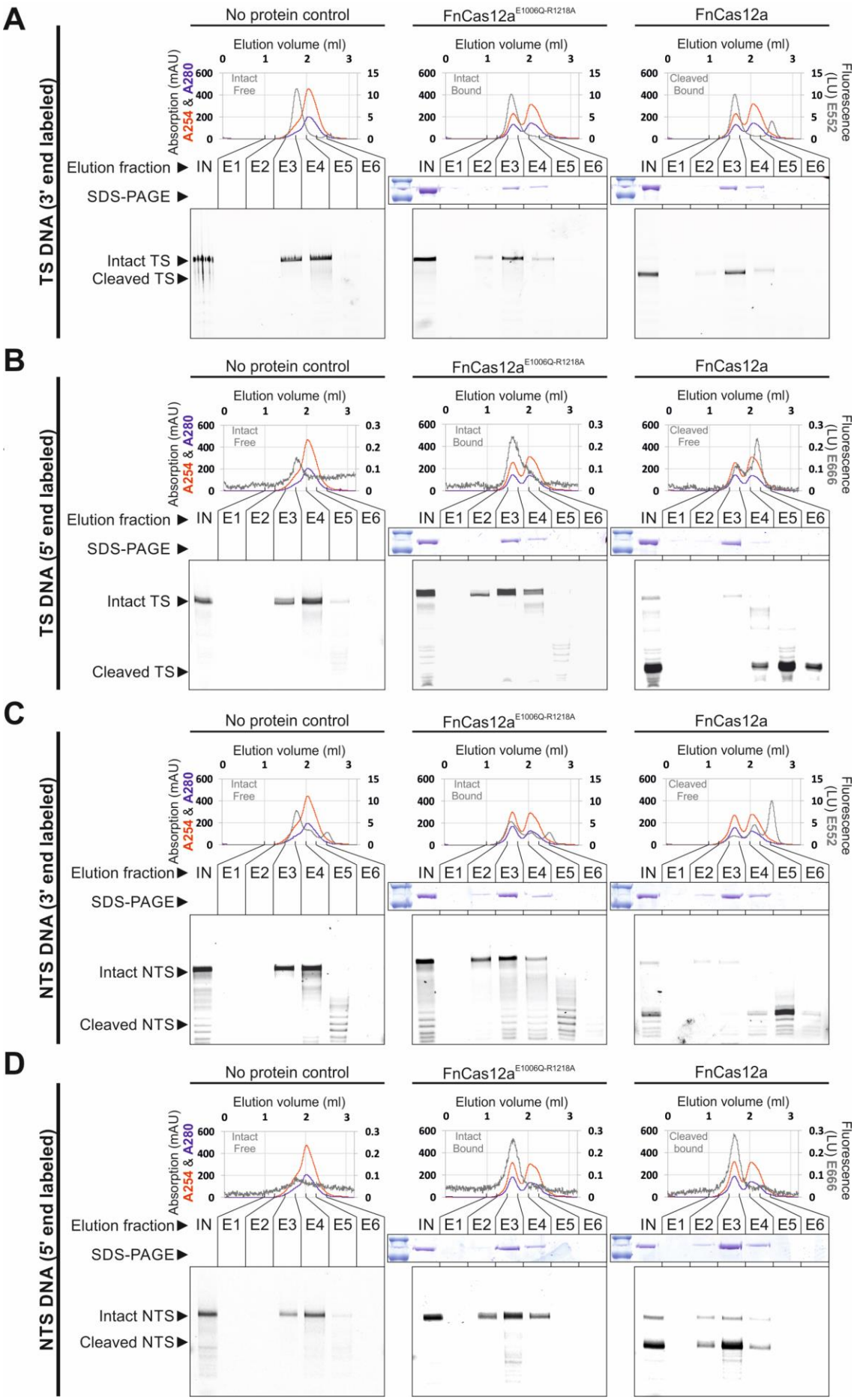

A
TS DNA (3' end labeled)
No protein control
FnCas12a E1006Q-R1218A
FnCas12a
Elution volume (ml)
Absorption (mAU) A254 & A280
Fluorescence (LU) E552
Intact Free
Intact Bound
Cleaved Bound
Elution fraction
IN E1 E2 E3 E4 E5 E6
SDS-PAGE
Intact TS
Cleaved TS
B
TS DNA (5' end labeled)
Fluorescence (LU) E666
Intact Free
Intact Bound
Cleaved Free
Intact TS
Cleaved TS
C
NTS DNA (3' end labeled)
Intact NTS
Cleaved NTS
D
NTS DNA (5' end labeled)
Cleaved bound

Figure S7. Fate of the DNA strands after Cas12a-crRNA mediated cleavage. Related to Figure 5

FnCas12a-crRNA or FnCas12a$^{E1006Q\text{-}R1218A}$-crRNA complexes were incubated with dsDNA targets containing fluorophore-labeled TS (panel A: TS 3' end labeled, panel B: TS 5' end labeled) or NTS (panel C: NTS 3' end labeled, panel B: NTS 5' end labeled) DNA and samples analyzed by fluorescence-detection size exclusion chromatography. Elution fractions were further analyzed for protein and fluorophore-labeled nucleic acid content by SDS-PAGE and 20% denaturing (7 M Urea) polyacrylamide gel analyses, respectively. IN: HPLC input; E1-6: Elution fractions; ctrl: Control sample containing catalytic mutant FnCas12a$^{E1006Q\text{-}R1218A}$ instead of FnCas12a.

Table S1. Oligonucleotides used in this study. Related to Figures 1-5

	Oligo	Sequence (5'-3')	Description
RNA	crRNA1	AAUUUCUACUGUUGUAGAUAGAUUAAAAGGUAAUUCUAUCUUG	crRNA
	crRNA-λ	AAUUUCUACUGUUGUAGAUGUGAUAAGUGGAAUGCCAUGUGGG	crRNA
DNA ligands	oDS141	AGTCCTTTATCTAATTTTCCATTAAGATAGAACTATGC	Non-target strand
	oDS142	ATAGTTCATAGAATTACCTTTTAATCTTAAAGGACTGC	Target strand
	oDS311	ATAGAATTACCTTTTAATCT	ssDNA TS
M13 *trans*-cleavage	oDS302	GCCTATCCCTATGACGTGCC	Non-comp. ssDNA
	oDS311	ATAGAATTACCTTTTAATCT	Comp. ssDNA
	oDS339	ATAGAATTACCTTTTAATCTTAAAT	Comp. ds TS
	oDS340	ATTTAAGATTAAAAGGTAATTCTAT	Comp. ds NTS
FQ-reporter *trans*-cleavage DNA targets	oDS343	CAGATCTCAACAAGATAGAATTACCTTTTAATCTACGCTTATTAGAA	TS1-PAM
	oDS344	TTCTAATAAGCGTAGATTAAAAGGTAATTCTATCTTGTTGAGATCTG	NTS1-PAM
	oDS345	CAGATCTCAACAAGATAGAATTACCTTTTAATCTTCGCTTATTAGAA	TS1+1PAM
	oDS346	TTCTAATAAGCGAAGATTAAAAGGTAATTCTATCTTGTTGAGATCTG	NTS1+1PAM
	oDS347	CAGATCTCAACAAGATAGAATTACCTTTTAATCTTAGCTTATTAGAA	TS1+2PAM
	oDS348	TTCTAATAAGCTAAGATTAAAAGGTAATTCTATCTTGTTGAGATCTG	NTS1+2PAM
	oDS349	CAGATCTCAACAAGATAGAATTACCTTTTAATCTTAACTTATTAGAA	TS1+3PAM
	oDS350	TTCTAATAAGTTAAGATTAAAAGGTAATTCTATCTTGTTGAGATCTG	NTS1+3PAM
	oDS351	CAGATCTCAACAAGATAGAATTACCTTTTAATCTTAAATTATTAGAA	TS1+4PAM
	oDS352	TTCTAATAATTTAAGATTAAAAGGTAATTCTATCTTGTTGAGATCTG	NTS1+4PAM
FQ-reporter *trans*-cleavage DNA targets	oDS270	ACTCAATTTTGACAGCCCACATGGCATTCCACTTATCACTAAAGGCATCCTTCCACGT	TS2+4PAM
	oDS271	ACGTGGAAGGATGCCTTTAGTGATAAGTGGAATGCCATGTGGGCTGTCAAAATTGAGT	NTS2+4PAM
	oDS356	ACTCAATTTTGACAGCCCACATGGCATTCCACTTATCACACGCGGCATCCTTCCACGT	TS2-PAM
	oDS357	ACGTGGAAGGATGCCGCGTGTGATAAGTGGAATGCCATGTGGGCTGTCAAAATTGAGT	NTS2-PAM
	oDS370	ACTCAATTTTGACAGCCCACATGGCATTCCACTTATCACTCGCGGCATCCTTCCACGT	TS2+1PAM
	oDS371	ACGTGGAAGGATGCCGCGAGTGATAAGTGGAATGCCATGTGGGCTGTCAAAATTGAGT	NTS2+1PAM
	oDS372	ACTCAATTTTGACAGCCCACATGGCATTCCACTTATCACTAGCGGCATCCTTCCACGT	TS2+2PAM
	oDS373	ACGTGGAAGGATGCCGCTAGTGATAAGTGGAATGCCATGTGGGCTGTCAAAATTGAGT	NTS2+2PAM
	oDS374	ACTCAATTTTGACAGCCCACATGGCATTCCACTTATCACTAACGGCATCCTTCCACGT	TS2+3PAM
	oDS375	ACGTGGAAGGATGCCGTTAGTGATAAGTGGAATGCCATGTGGGCTGTCAAAATTGAGT	NTS2+3PAM
FQ-reporter *trans*-cleavage DNA targets	oDS270	ACTCAATTTTGACAGCCCACATGGCATTCCACTTATCACTAAAGGCATCCTTCCACGT	TS3+PAM
	oDS271	ACGTGGAAGGATGCCTTTAGTGATAAGTGGAATGCCATGTGGGCTGTCAAAATTGAGT	NTS3+PAM
	oDS358	ACGTGGAAGGATGCCTTTACACTATTCACCTTACGGTACACCCCTGTCAAAATTGAGT	NTS3+PAM unwDNA
	oDS356	ACTCAATTTTGACAGCCCACATGGCATTCCACTTATCACACGCGGCATCCTTCCACGT	TS3-PAM
	oDS357	ACGTGGAAGGATGCCGCGTGTGATAAGTGGAATGCCATGTGGGCTGTCAAAATTGAGT	NTS3-PAM
	oDS359	ACGTGGAAGGATGCCGCGTCACTATTCACCTTACGGTACACCCCTGTCAAAATTGAGT	NTS3-PAM unwDNA
Cis-cleavage of pre-unwound dsDNA targets	oDS272	Cy5-ACTCAATTTTGACAGCCCACATGGCAT TCCACTTATCACTAAAGGCATCCTTCCACGT	TS3+PAM 5' Cy5
	oDS271	ACGTGGAAGGATGCCTTTAGTGATAAGTGGAATGCCATGTGGGCTGTCAAAATTGAGT	NTS3+PAM
	oDS358	ACGTGGAAGGATGCCTTTACACTATTCACCTTACGGTACACCCCTGTCAAAATTGAGT	NTS3+PAM unwDNA
	oDS363	Cy5-ACTCAATTTTGACAGCCCACATGGCAT TCCACTTATCACACGCGGCATCCTTCCACGT	TS3-PAM 5' Cy5
	oDS356	ACTCAATTTTGACAGCCCACATGGCATTCCACTTATCACACGCGGCATCCTTCCACGT	TS3-PAM
	oDS357	ACGTGGAAGGATGCCGCGTGTGATAAGTGGAATGCCATGTGGGCTGTCAAAATTGAGT	NTS3-PAM
	oDS359	ACGTGGAAGGATGCCGCGTCACTATTCACCTTACGGTACACCCCTGTCAAAATTGAGT	NTS3-PAM unwDNA

Cy5, ATTO532: Fluorescent labels Cyanine 5, ATTO532. *: Phosphorothioate modification.

Table S1 (continued). Oligonucleotides used in this study. Related to Figure 1-5

	Oligo	Sequence (5'-3')	Description
FnCas12a mutants expression vector cloning	oDS366	TTTCCCCTCCTGATTATTTTTTATCC	Gibson cloning pDS117 RV
	oDS367	GAAGAGTATTTTGAGTTCGTACAAAAT	Gibson cloning pDS117 FW
	oDS368	AAACCCAAAATTCAGATCCTCAAAAA	Gibson cloning pDS116 RV
	oDS369	CAGACAGGTATTATATACTATGTCC	Gibson cloning pDS116 FW
	gbDS02	GAGGATCTGAATTTTGGGTTTAAAGCTGGGGCATTCAAGGTCGAGAAGCAAGTATATC AGAAGCTGGAAAAAATGTTAATTGAGAAATTAAACTATTTAGTTTTCAAAGATAATGA GTTTGATAAAACCGGGGGGGGTATTACGTGCATATCAATTAACAGCTCCGTTTGAGACC TTTAAAGCGATGGGTGCACAGACAGGTATTATATACTATG	gBlock insert for pDS116
	oDS364	AAAAATAATCAGGAGGGGAAAGCACTAAATCTCGTTATAGCAGCTGAAGAGTATTTTG AGTTCGTAC	FW insert for pDS117
	oDS365	GTACGAACTCAAAATACTCTTCAGCTGCTATAACGAGATTTAGTGCTTTCCCCTCCTG ATTATTTTT	RV insert for pDS117
Order of strand cleavage experiment	oDS270	ACTCAATTTTGACAGCCCACATGGCATTCCACTTATCACTAAAGGCATCCTTCCACGT	λ TS
	oDS271	ACGTGGAAGGATGCCTTTAGTGATAAGTGGAATGCCATGTGGGCTGTCAAAATTGAGT	λ NTS
	oDS272	Cy5-ACTCAATTTTGACAGCCCACATGGCAT TCCACTTATCACTAAAGGCATCCTTCCACGT	λ TS 5' Cy5
	oDS273	Cy5-ACGTGGAAGGATGCCTTTAGTGATAAG TGGAATGCCATGTGGGCTGTCAAAATTGAGT	λ NTS 5' Cy5
	oDS307	ACTCAATTTTGA*C*A*G*C*C*C*A*C*A*T*GGCATTCCACTTATCACTAAAGGCA TCCTTCCACGT	λ TS modified
	oDS308	ACGTGGAAGGATGCCTTTAGTGATAAGTG*G*A*A*T*G*C*C*A*T*G*T*G*GGCT GTCAAAATTGAGT	λ NTS modified
	oDS353	ACGTGGAAGGATGCCTTTAGTGATAAGTG*G*A*A*T*G*C*C*A	λ NTS truncated
	oDS353	ACGTGGAAGGATGCCTTTAGTGATAAGTG*G*A*A*T*G*C*C*A	λ NTS Nicked1
	oDS354	T*G*T*G*GGCTGTCAAAATTGAGT	λ NTS Nicked2
	oDS355	ACGTGGAAGGATGCCTTTAGTGATAAGTG*G*A*A*T*G*C*C*AT*G*T*G*GGCTG TCAAAATTGAGT	λ NTS cleavable
	oDS362	ACGTGGAAGGATGCCTTTAGTGATAAGTC*C*T*T*A*C*G*G*T*A*C*A*C*C*C* G*A*C*TGTTTTAACTCA	λ NTS unwound
Target release experiments	oDS270	ACTCAATTTTGACAGCCCACATGGCATTCCACTTATCACTAAAGGCATCCTTCCACGT	λ TS
	oDS271	ACGTGGAAGGATGCCTTTAGTGATAAGTGGAATGCCATGTGGGCTGTCAAAATTGAGT	λ NTS
	oDS272	Cy5-ACTCAATTTTGACAGCCCACATGGCAT TCCACTTATCACTAAAGGCATCCTTCCACGT	λ TS 5' Cy5
	oDS273	Cy5-ACGTGGAAGGATGCCTTTAGTGATAAG TGGAATGCCATGTGGGCTGTCAAAATTGAGT	λ NTS 5' Cy5
	oDS287	ACTCAATTTTGACAGCCCACATGGCATTCCACTTATCACTAAAGGCATCCTTCCACGT -ATTO532	λ TS 3' ATTO532
	oDS288	ACGTGGAAGGATGCCTTTAGTGATAAGTGGAATGCCATGTGGGCTGTCAAAATTGAGT -ATTO532	λ NTS 3' ATTO532

Cy5, ATTO532: Fluorescent labels Cyanine 5, ATTO532. *: Phosphorothioate modification.

Table S2. Plasmids used in this study. Related to Figure 1-5

Plasmid	Description	Source
pDS015	*F. novicida cas12a* with N-term. His-tag and TEV site in pML-1B. Expression vector for FnCas12a.	(Swarts et al., 2017)
pDS069	Like pDS015, but with FnCas12a mutation E1006Q	(Swarts et al., 2017)
pDS073	Like pDS015, but with FnCas12a mutations E1006Q and R1218A	(Swarts et al., 2017)
pDS116	Like pDS015, but with FnCas12a mutations K1281A, K1287A, and N1288A	This study
pDS117	Like pDS015, but with FnCas12a mutations R1014A, R016A, K1066A, and K1069A	This study
M13mp18	Single stranded M13 DNA	New England Biolabs
M13mp18 RF I	Double stranded M13 DNA	New England Biolabs